remote sensing

MDPI

Article

A Comprehensive Assessment of Multiple High-Resolution Precipitation Grid Products for Monitoring Heavy Rainfall during the "7.20" Extreme Rainstorm Event in China

Zihao Pang [1], Yu Zhang [2], Chunxiang Shi [1,*], Junxia Gu [1], Qingjun Yang [3], Yang Pan [1], Zheng Wang [1] and Bin Xu [1]

[1] National Meteorological Information Center, Beijing 100081, China; pangzh@cma.gov.cn (Z.P.); gujx@cma.gov.cn (J.G.); pany@cma.gov.cn (Y.P.); wangz@cma.gov.cn (Z.W.); xub@cma.gov.cn (B.X.)
[2] Henan Meteorological Observation Data Center, Zhengzhou 450003, China; zhangyuc477201@cma.cn
[3] Qinghai Meteorological Information Center, Xining 810012, China; yangqingjun282117@cma.cn
* Correspondence: shicx@cma.gov.cn

Abstract: Precipitation products play an important role in monitoring rainstorm processes. This study takes a rare historical event of extreme, heavy precipitation that occurred in Henan Province, China, in July 2021 as a research case. By analyzing the distribution of the spatial and temporal characteristics of precipitation errors, using a probability density function of the occurrence of precipitation and the daily variation pattern, we assess the capability of a radar precipitation estimation product (RADAR), satellite precipitation products (IMERG and GSMAP), a reanalysis product (ERA5) and a precipitation fusion product (the CMPAS) to monitor an extreme rainstorm in the Henan region. The CMPAS has the best fit with the gauge observations in terms of the precipitation area, precipitation maximum and the evolution of the whole process, with a low spatial variability of errors. However, the CMPAS slightly underestimated the precipitation extremum at the peak moment (06:00–08:00). The RADAR product was prone to a spurious overestimation of the originally small rainfall, especially during peak precipitation times, with deviations concentrated in the core precipitation area. The IMERG, GSMAP and ERA5 products have similar performances, all of which failed to effectively capture heavy precipitation in excess of 60 mm/h, with negative deviations in precipitation at mountainfront locations west of northern Henan Province. There is still a need for terrain-specific error revisions for areas with large topographic relief. By merging and processing precipitation data from multiple sources, the accuracy of the CMPAS is better than any single-source precipitation product. The CMPAS has the characteristic advantage of high spatial and temporal resolutions (0.01° × 0.01°/1 h), which play a positive role in precipitation dynamic monitoring, providing early warnings of heavy rainfall processes and hydrological application research.

Keywords: extreme rainstorm; radar; satellite; ERA5; multi-source data merging; precipitation monitoring; error characteristics

Citation: Pang, Z.; Zhang, Y.; Shi, C.; Gu, J.; Yang, Q.; Pan, Y.; Wang, Z.; Xu, B. A Comprehensive Assessment of Multiple High-Resolution Precipitation Grid Products for Monitoring Heavy Rainfall during the "7.20" Extreme Rainstorm Event in China. *Remote Sens.* **2023**, *15*, 5255. https://doi.org/10.3390/rs15215255

Academic Editors: Ehsan Sharifi and Vincenzo Levizzani

Received: 4 September 2023
Revised: 29 October 2023
Accepted: 1 November 2023
Published: 6 November 2023

1. Introduction

Precipitation is an important component of global water and energy cycles and plays an important part in the interactions among the hydrosphere, atmosphere and biosphere [1]. Accurate precipitation data are essential in hydrological, meteorological and ecological research [2–4]. In the current context of global warming, there is an increasing trend of extreme rainfall events [5]. In both rural and urban areas of China, a notable decline in light rainfall has been observed, accompanied by an increase in heavy precipitation events [6]. The frequency of extreme hourly precipitation nationwide has shown an increase of 0.7 h/10a; however, the overall trend in precipitation intensity remains insignificant across the country [7]. Liu et al. [8] also emphasized an increased risk of extreme wet and hot events in different regions of China. From 17 to 22 July 2021, Henan Province experienced a historically rare extreme, heavy precipitation event (referred to as the "7.20"

Henan rainstorm), with rainfall in the Hebi area reaching 1122.6 mm. The maximum hourly rainfall at Zhengzhou station reached 201.9 mm, exceeding the historical extreme value for mainland China and causing significant casualties and damage to property [9]. This extraordinary rainstorm process occurred against a background of weak weather-scale system forcing, and the coupling of low-level jet streams provided good convergence–divergence forcing for heavy precipitation [10]. The joint influence of strong and stable Typhoon In-Fa and a stable atmospheric circulation situation in the middle and high latitudes established long-range water-vapor transport channels [11]. The combined effect of the upper-level divergence circulation and the blocking uplift of the mountains induced a deep, meso-β-scale convective vortex system, producing extremely intense precipitation [12]. Henan Province is located in the mid-latitude north–south climate transition zone and has a complex topography; there have been many heavy rain disasters in Henan Province throughout history, such as the 58.7, 75.8, 82.8, 96.8 and 18.8 extreme events [13]. Therefore, in the Henan region, there is a great need for accurate and reliable real-time quantitative precipitation grid products to dynamically monitor the whole process of the occurrence and development of precipitation, providing effective supportive information for disaster warnings and decision-making services while further improving the effectiveness of short-range forecasting and reducing the damage caused by heavy rainfall and flooding.

The quantitative precipitation datasets currently available on a regional scale in China mainly originate from gauge observations, weather radar, satellite measurements, reanalysis data and multi-source-observation precipitation fusion products. Gauge observations are considered the most accurate observations of precipitation but cannot effectively reflect the spatial distribution of extreme precipitation events due to the uneven distribution and varying density of gauge sites [14,15]. Ground-based meteorological radar systems and space-based meteorological satellites are the two main observation techniques for the remote sensing of precipitation [16]. Significant developments have been made in quantitative techniques for the estimation of precipitation from radar data, including the establishment of Z-I relationships from radar, radar puzzle studies and estimated precipitation revisions from joint ground-based observations [17–19]. However, quantitative radar precipitation estimates have some drawbacks, such as their limited spatial coverage, the occlusion of radar signals by terrain, radar ray lifting and uncertainty in the Z-R relationship [20]. Satellite remote sensing is currently the only method of obtaining global-scale precipitation observations [1].

The Global Precipitation Measurement (GPM) program is a new generation of global precipitation-observation satellites developed jointly by the National Aeronautics and Space Administration (NASA) and the Japan Aerospace Exploration Agency (JAXA). The GPM program uses advanced, dual-band rain-measuring radar and microwave sensors and continually improving inversion algorithms. IMERG is a NASA release that participates in the GPM program to obtain level 3 products, and JAXA developed the GSMAP global precipitation dataset using satellite sensor data from the GPM observing platform. Although both IMERG and GSMAP are new-generation global precipitation datasets with high spatial and temporal resolutions, they still have problems, such as insufficient inversion accuracy for small and extreme precipitation events, large errors in precipitation products at high altitudes and high latitudes and the overestimation of precipitation in inland water bodies [21–23]. Precipitation data from atmospheric reanalysis datasets are often used to analyze the spatial and temporal characteristics of precipitation. ERA5 is a fifth-generation reanalysis product from the European Centre for Medium-Range Weather Forecasts (ECMWF). The data are based on an improved 3D variational technique and have the advantages of high spatial and temporal resolutions, fast updates and a wide range of parameters, which have attracted a significant amount of attention. However, the atmospheric reanalysis data are the product of the fusion of numerical forecast products and observations. The errors in these forecast products and observations mean that assimilation methods affect the quality of the reanalysis of climate data [24–26].

In contrast, precipitation fusion products fully combine the advantages of precipitation data from different sources and have been widely used in weather and climate monitoring, climate change research, model forecast testing and hydrological forecasting [27,28]. The National Meteorological Information Center of China has continuously developed and improved data fusion technology to create the Chinese multi-source observation precipitation fusion product (CMPAS), which has spatial and temporal resolution of 1 h/0.01°. The data sources for this product include hourly precipitation information from nearly 50,000 automatic weather stations in China, quantitative radar precipitation estimation products and CMORPH satellite inversion precipitation data [29,30]. The CMPAS exhibits better accuracy than any single-source precipitation product, especially in areas with sparse gauges [31,32].

There have been some studies examining the ability of various precipitation products to capture extreme precipitation events [33–35]. However, there is still uncertainty in their ability to accurately capture heavy rainfall, and this uncertainty varies depending on factors such as precipitation level and region. Therefore, further research is needed to assess the ability of different precipitation products to monitor the exceptionally heavy rainfall event in Henan. This study uses the "7.20" Henan rainstorm event as the research object, employing dense gauge observations as the reference to evaluate whether RADAR, IMERG product, GSMAP, ERA5 and CMPAS can accurately and reasonably portray the distribution characteristics and evolution process of the extreme precipitation event through various error analysis indicators. This work is significant as it provides valuable feedback to product developers and useful information for end-users by analyzing the error and uncertainty in precipitation products.

2. Data and Methods

2.1. Study Area

Henan Province is located in the mid-latitude north–south climate transition zone. Rolling hills and mountains are found to the west, while the vast East Henan Plain lies to the east. Topographic uplift results in most rainstorms being concentrated in the mountainous area on the windward slopes of the Taihang Mountains, leading to highly uneven seasonal and regional distribution of rainfall, and sudden heavy downpours can cause serious secondary disasters. Henan experiences frequent heavy rainfall from June to August every year as a result of the seasonal northward movement and southward retreat of the subtropical high-pressure region. Low vortex shear lines and typhoon weather systems contribute to extreme heavy precipitation events in Henan [36]. The whole study area (Figure 1) is at 31°N–40°N latitude and 109°E–112°E longitude, with a core area of precipitation at at 34°N–36.7°N latitude and 112.5°E–114.8°E longitude. The study period extends from 00:00 UTC on 17 July to 23:00 UTC on 22 July 2021.

2.2. Data

2.2.1. Rain Gauge Observations

Rain gauge observations are typically considered the most accurate source of precipitation data and play a crucial role in quantitative studies of surface precipitation [37]. Hourly precipitation data from approximately 11,000 automatic weather stations in Henan Province and the surrounding area in July 2021 are used to evaluate the accuracy of precipitation grid products during the "7.20" Henan rainstorm event. Figure 1b illustrates the spatial distribution of the station locations and their ground elevation. The station observations are densely distributed, providing a reliable spatial representation of the precipitation. The precipitation data from the automatic weather stations undergo strict operational quality control [38], including boundary value checks, temporal consistency checks and spatial consistency checks, with a minimum detectable precipitation of 0.1 mm/h.

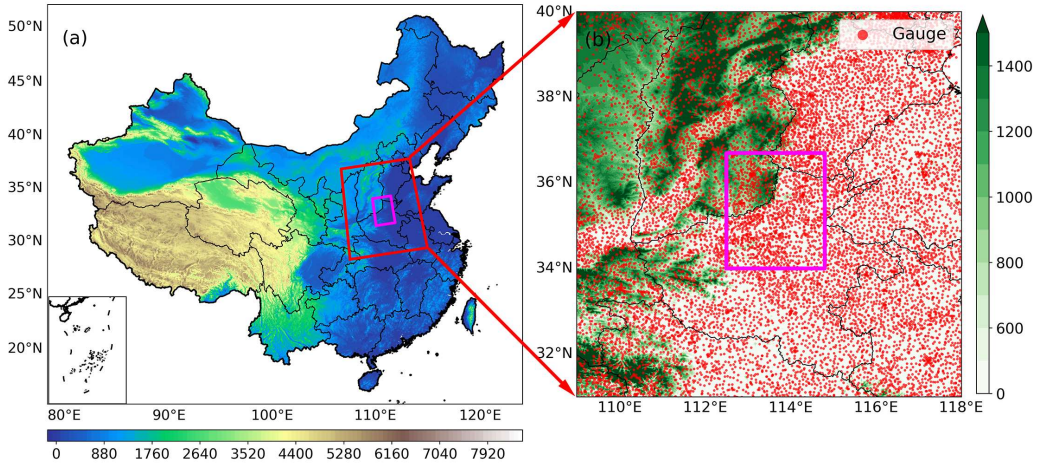

Figure 1. (**a**) Map of the national administrative divisions in China; the area circled in red is the study area, and the purple line shows the core area of precipitation; the filled part is the topographic height description (unit: m). (**b**) Spatial distribution of the gauges (red points) and the topographic features (filled part, unit: m) within the study area (31–40°N, 109–112°E), and the purple line shows the core area of precipitation.

2.2.2. RADAR Product

The RADAR precipitation product is derived from radar observation data developed by Meteorological Detection Center of China Meteorological Administration. The RADAR product estimates precipitation based on a real-time statistical Reflectivity Factor–Rain Intensity relationship from a networked radar and is calibrated using precipitation data from 2400 national weather stations through Kalman filtering and average calibration. The spatial and temporal resolution of the product is 1 h/0.01° [39].

2.2.3. IMERG Product

The IMERG currently provides three types of satellite precipitation data with a spatial and temporal resolution of 0.1°/30 min: EarlyRun, LateRun and FinalRun. Both the EarlyRun and LateRun are near-real-time products, released with 4 h delay and 12 h delay, respectively. The EarlyRun uses only forward propagation (equivalent to extrapolation) algorithms, while the LateRun utilizes both forward and backward propagation (allowing interpolation). The FinalRun product is calibrated using global rainfall stations and is more accurate than the EarlyRun and LateRun products in terms of accuracy; however, the data from the FinalRun product is released with a delay of about 3.5 months [40]. The data used in this study is FinalRun product.

2.2.4. GSMAP Product

The GSMAP utilizes microwave datasets provided by low earth orbit satellite observations and visible/infrared datasets provided by geosynchronous satellite observations as the input sources for the inversion algorithm. The source data are processed using cloud motion vector and Kalman filtering methods, resulting in three different remote sensing precipitation data products: GSMAP_NRT, GSMAP_MVK and GSMAP_Gauge. The near-real-time data product, GSMAP_NRT, employs a forward cloud vector motion scheme during processing, while the standard product, GSMAP_MVK, utilizes a bi-directional (forward and backward) cloud vector motion scheme. GSMAP_Gauge is a calibrated version of GSMAP_MVK based on observations from the Climate Prediction Center (CPC) global surface rainfall stations [41]. The data used in this study is obtained from GSMAP_Gauge with a spatial and temporal resolution of 1 h/0.01°.

2.2.5. ERA5 Product

The ERA5 reanalysis dataset, released in July 2017, is the fifth generation of global climate products produced by the ECMWF and represents a significant upgrade from the previous generation of the ERA-Interim dataset. The precipitation data has been widely utilized in meteorological and hydrological research, leading to numerous meaningful results. Although the ERA5 reanalysis precipitation dataset has shown considerable improvement compared to the ERA-Interim dataset, it still contains large errors in areas dominated by convective storms [42].

2.2.6. CMPAS Product

The CMPAS product is produced by China multi-source precipitation analysis system, developed by the National Meteorological Information Center of the CMA (China Meteorological Administration). It uses probability density function (PDF), optimum interpolation method (OI) and Bayesian model averaging method (BMA), combined with high-density gauge precipitation observations, high-resolution weather radar quantitative precipitation estimation (QPE) and satellite-based precipitation estimation, to generate gauge-radar-satellite merged hourly precipitation product [43–45]. In December 2016, the Chinese multi-source observation precipitation fusion product (CMPAS) entered operational trials with a spatial and temporal resolution of 1 h/0.01° and was released in real time through the China Meteorological Data Network, the National Meteorological Data Intranet and the China Meteorological Administration Satellite Broadcasting System (CMACast). Currently, the CMPAS plays an active role in meteorological operations such as forecasting and meteorological disaster warnings [45].

2.3. Methods

2.3.1. Data Pre-Processing

Rain gauge observations represent station data, while CMPAS, RADAR, IMERG, GSMAP and ERA5 provide grid data. Rain gauge observations differ from various precipitation products in terms of data type and spatial–temporal scale; therefore, data preprocessing is necessary. Both rain gauge observations and CMPAS, RADAR, GSMAP, ERA5 contain hourly-scale data. It is essential to standardize the half-hourly estimated data from IMERG into hourly intervals. Regarding spatial matching, since there are uncertainties when interpolating rain gauge data onto the grid system, we employ a point-to-point analysis method to match the grid data with the stations. The nearest value from the grid points to each station is selected for comparison with the gauge observation. Subsequently, corresponding grid precipitation data are extracted at each rain gauge station location to complete sample matching between the grid precipitation and gauge measurements [46].

2.3.2. Assessment Indicators

Several statistical metrics are utilized for quantifying and comparing the performance of different types of precipitation products, which include the mean error (ME), relative bias (rBIAS), root-mean-square error (RMSE), correlation coefficient (CORR) [47] and Kling–Gupta efficiency (KGE). The detailed calculation of these indicators is as follows.

$$\mathrm{ME} = \frac{1}{n}\sum_{i=1}^{n}(y_i - x_i), \tag{1}$$

$$\mathrm{rBIAS} = \sum_{i=1}^{n}(y_i - x_i) / \sum_{i=1}^{n} x_i, \tag{2}$$

$$\mathrm{RMSE} = \sqrt{\sum_{i=1}^{n}\frac{(y_i - x_i)^2}{n}}, \tag{3}$$

$$\mathrm{CORR} = \frac{\sum_{i=1}^{n}(y_i - \overline{y})(x_i - \overline{x})}{\sqrt{\sum_{i=1}^{n}(y_i - \overline{y})^2 \sum_{i=1}^{n}(x_i - \overline{x})^2}}, \quad (4)$$

$$\mathrm{KGE} = 1 - \sqrt{(r-1)^2 + (\beta - 1)^2 + (\gamma - 1)^2} \quad (5)$$

where n is the total number of samples and y and x represent the precipitation product samples and the gauge samples, respectively. rBIAS is dimensionless and is used to measure the deviation of the precipitation products from the rain gauge observations. When multiplied by 100, rBIAS expresses the degree of overestimation or underestimation as a percentage. CORR is used to quantify the correlation of the precipitation products with the rain gauge observations. KGE is an objective performance metric that combines the correlation, the deviation (Bias, β) and the variability (VAR, γ). The deviation $\beta = \frac{\mu_G}{\mu_O}$ is the ratio of estimated and observed means, where μ is the average value. The variability $\gamma = \frac{\sigma_G/\mu_G}{\sigma_O/\mu_O}$ is the ratio of the estimated and observed coefficients of variation, and σ is the standard deviation.

In practical applications, we also need to consider the ability of the precipitation products to capture rainfall events. We use the Probability of Detection (POD), False Alarm Rate (FAR), Frequency Bias Index (FBI) and TS score to analyze the agreement between observed rainfall events and estimated events using precipitation products [48]. The equations for each evaluation index are as follows.

$$\mathrm{POD} = \frac{\mathrm{H}}{\mathrm{H} + \mathrm{M}}, \quad (6)$$

$$\mathrm{FAR} = \frac{\mathrm{F}}{\mathrm{H} + \mathrm{F}}, \quad (7)$$

$$\mathrm{FBI} = \frac{\mathrm{H} + \mathrm{F}}{\mathrm{H} + \mathrm{M}}, \quad (8)$$

$$\mathrm{TS} = \frac{\mathrm{H}}{\mathrm{H} + \mathrm{F} + \mathrm{M}} \quad (9)$$

where H (hits) is the frequency of rain observed simultaneously by the precipitation product and the rain gauge; F (false Alarm) is the frequency of precipitation product with rain but no rain observed by gauge; and M (misses) is the frequency of gauge with rain but no rain observed by precipitation product. This paper also utilizes the cumulative distribution function (CDF), which is the integral of the probability density function (PDF). It serves as a model for determining the probability of a random variable assuming values below a specific threshold. CDFc represents the cumulative probability function of precipitation coincidence, while CDFc represents the cumulative probability function of precipitation volume. Five different ranges are defined to discriminate between different intensities of rainfall in order to evaluate combined performance: light rain (0.1–2 m/h), moderate rain (2–5 mm/h), heavy rain (5–10 mm/h), rainstorm (10–20 mm/h) and heavy rainstorm (>20 mm/h).

3. Results

3.1. Spatial Distribution Characteristics of Precipitation

The "7.20" Henan rainstorm is characterized by its long duration, extreme intensity of precipitation and record-breaking cumulated precipitation. The reasons for the formation of this extreme rainstorm are complex. The stable atmospheric circulation, sufficient water vapor and energy, topographic effects and long-term maintenance of convection systems in Henan are the major causes [6]. Figure 2 shows that precipitation is concentrated in northwestern central Henan, where the topography is significantly elevated (Figure 1b). Water vapor transported from the east and south is blocked by the topography and accumulates

in this region, resulting in an extreme precipitation event [49]. A comparison between accumulated precipitation from CMPAS, RADAR, IMERG, GSMAP and ERA5 from 00:00 on July 17 to 23:00 on July 22 with high-density rain gauge observations reveals that all the precipitation products can reflect the occurrence of this extremely heavy rainstorm event. The CMPAS exhibits a high agreement with gauge observations, accurately depicting precipitation distribution patterns and effectively capturing the extreme value of heavy rainfall centers, thus accurately reproducing actual rainstorm conditions. The RADAR also shows a high degree of precipitation reduction but overestimates the regional extent and extreme values of the heavy precipitation center. The IMERG, GSMAP and ERA5 perform significantly worse than CMPAS and RADAR as they fail to reflect cumulative precipitation > 600 mm. Additionally, the location of the area with >400 mm of rain is shifted to the southeast in the IMERG and more to the northwest in the ERA5. The GSMAP does not indicate any area with >400 mm of rain.

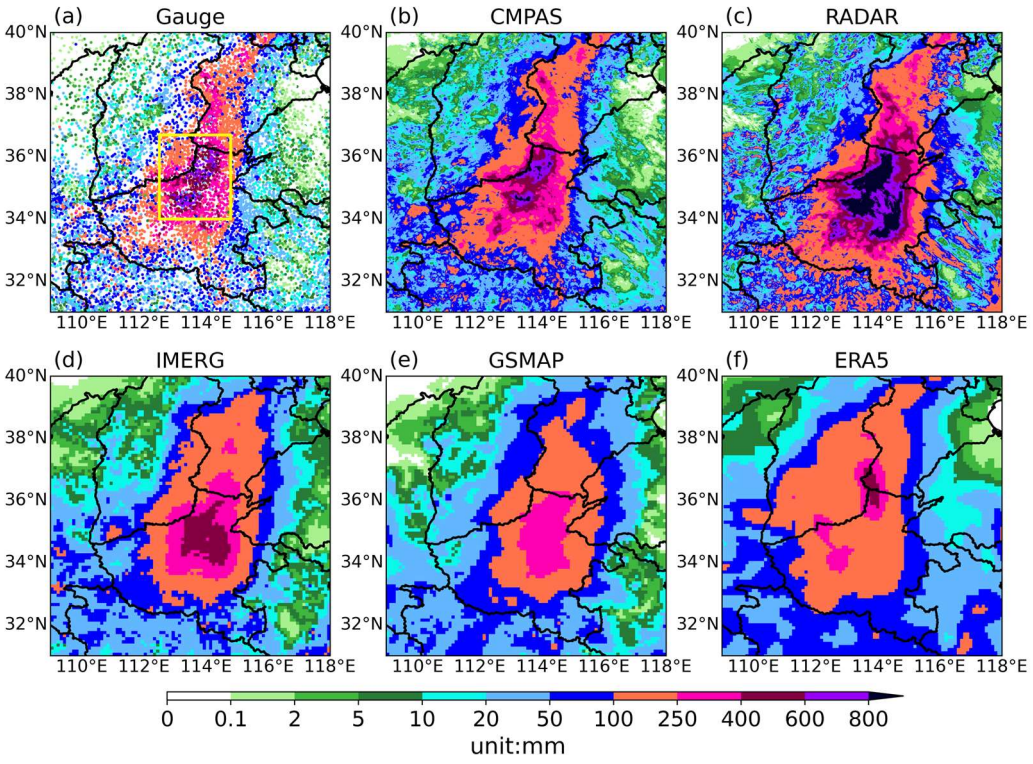

Figure 2. Spatial distribution of the accumulated precipitation (unit: mm) in the study area during the "7.20" Henan rainstorm compared with the original resolution of the gauge observations and various precipitation products: (**a**) gauge observations; (**b**) CMPAS; (**c**) RADAR; (**d**) IMERG; (**e**) GSMAP and (**f**) ERA5. The yellow box is the core area of precipitation.

Figure 3 is a scatter plot comparing the hourly rainfall between the rain gauges and precipitation products during the "7.20" Henan rainstorm, with a linear fit (red line). Warmer-colored scatter points indicate a larger precipitation sample size, while a black dashed line represents the 1:1 line of observations versus products. The results demonstrate that CMPAS exhibits the highest agreement with gauges, with the hourly precipitation evenly distributed around the 1:1 line and a linear slope of 0.924 for the scattered points. However, the fitted line is found to be right of the 1:1 line, suggesting that CMPAS may underestimate extremely heavy precipitation. The deviation of the linear fitted line of RADAR is larger, indicating that it is less accurate than the CMPAS in capturing extreme precipitation. The RADAR also shows false precipitation >100 m/h when no precipitation is recorded by rain gauges, which explains the overestimation of the cumulative precipitation by RADAR (Figure 2). The hourly precipitation of IMERG is concentrated at <60 mm/h, whereas that of GSMAP and ERA5 is concentrated at <25 mm/h and the linear fitted line

deviates from the 1:1 line. The poor ability of satellite products to capture precipitation extremes is related to the upper limit of the sensitivity of satellite sensors for remote sensing of precipitation [50]. The GMI sensor in the GPM detects precipitation up to only 60 mm/h. The ERA5 is limited by constraints in its convective parameterization scheme, resulting in an inability to effectively capture convective precipitation and poor performance in simulating heavy rainfall [51]. SUN et al. [52] proposed using machine learning techniques to correct ERA5's precipitation, making it more consistent with real conditions.

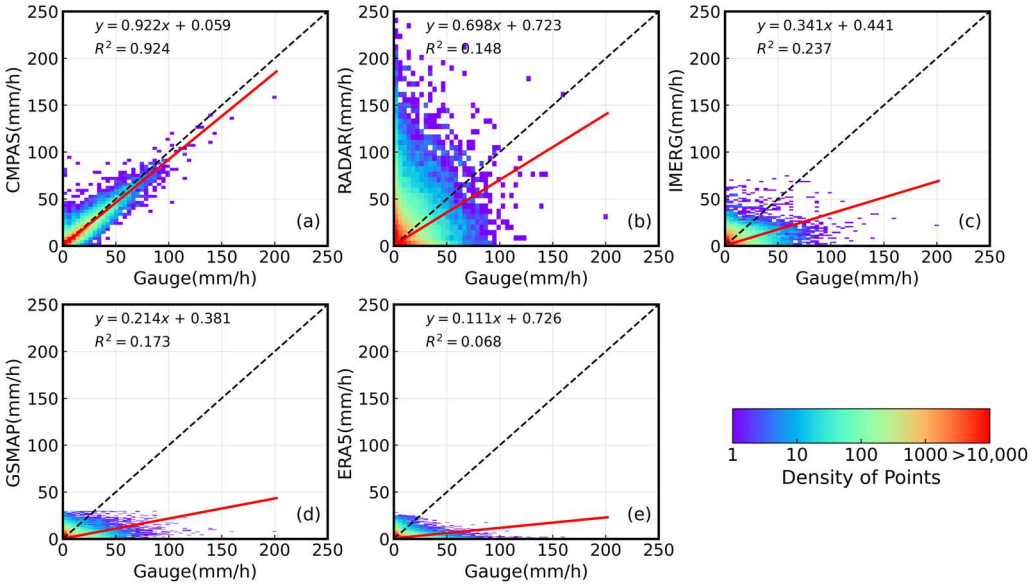

Figure 3. Scatterplot of the hourly rainfall (unit: mm/h) recorded by gauge observations and various precipitation products during the "7.20" Henan rainstorm and their linear regression fits (red lines) for (**a**) CMPAS, (**b**) RADAR, (**c**) IMERG, (**d**) GSMAP and (**e**) ERA5.

A comparative analysis of the spatial distribution of several evaluation indicators has been provided (Figures 4 and 5). The CMPAS outperforms other precipitation products significantly in all scoring indicators, with a small spatial variability of the precipitation deviation, indicating a consistent quality of CMPAS across the region. The ME of CMPAS is $\pm$0.05 mm/h, the RMSE is <1.5 mm/h in the core area of precipitation and the correlation coefficient and TS score are >0.9. KGE is concentrated above 0.8, and the coefficient of variation is less than 1, indicating that CMPAS exhibits less variability in precipitation than gauges (Table 1). The RADAR, IMERG, GSMAP and ERA5 have similar spatial distribution of errors. The RADAR overestimates precipitation in all regions except northwestern Henan Province; its greatest overestimation occurred in central-eastern Henan Province, with rBIAS reaching 77.9%. The RADAR has poor KGE indicators due to high deviation bias, which reaches 1.779, indicating that RADAR is approximately 1.8 times gauge observations. The rBIAS of GSMAP is $-$21.63%, whereas the rBIAS of IMEGR is close to 0. This difference arises because the range of overestimate and underestimate of precipitation in the study area is generally consistent for IMERG, whereas GSMAP exhibits a larger area of underestimation. The ERA5 significantly underestimates precipitation in the core area and overestimates it in western Henan. The correlation coefficients of the four precipitation products, RADAR, IMGRG, GSMAP and ERA5, are significantly higher in the core precipitation area than in the peripheral region, reaching above 0.6. TS scores also indicate that as the intensity of precipitation increases, so does its accuracy across all products, suggesting their ability to capture this process accurately. Additionally, both satellite and model products share a common feature: an underestimation of precipitation in the western part of northern Henan Province (negative deviation in ME). This may be attributed to the relatively undulating topography of this mountainous region located

upstream from these areas, indicating a need for further correction regarding topographic errors within both satellite and model precipitation products [53].

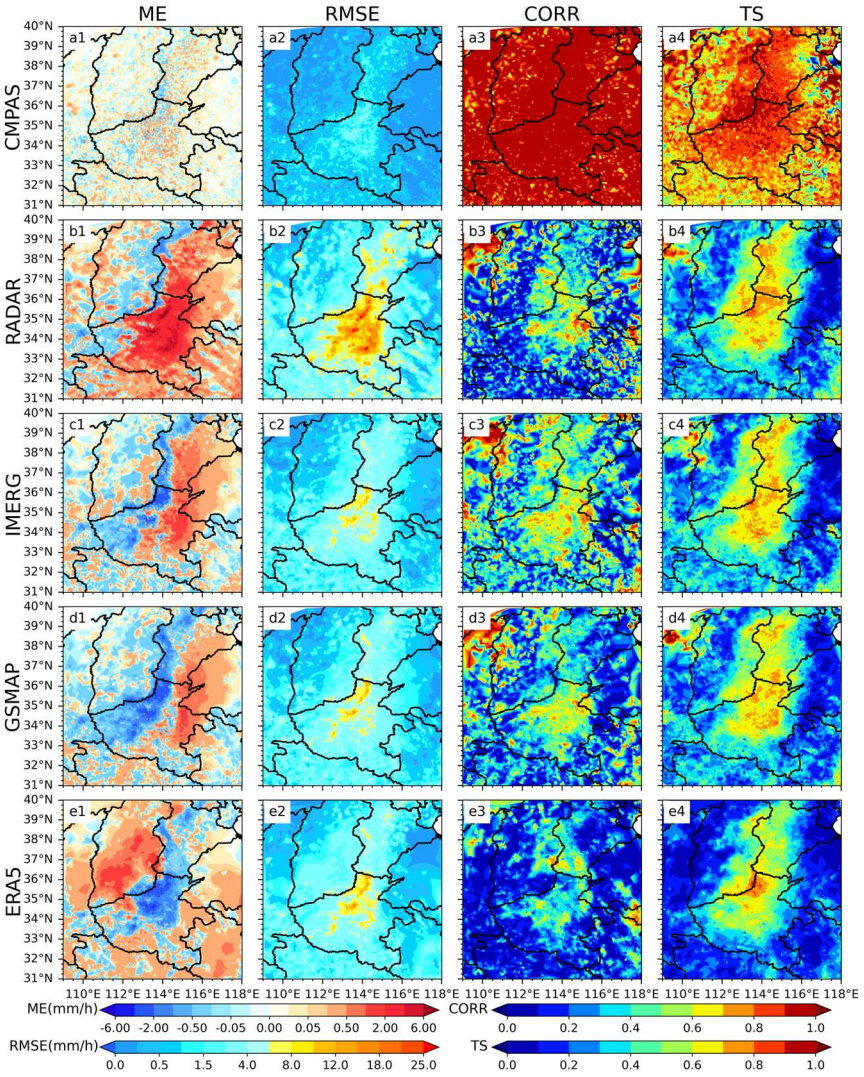

Figure 4. Spatial distribution of error indicators for various precipitation products during the "7.20" Henan rainstorm. (**a1**–**a4**) represent ME, RMSE, CORR and TS scores of CMPAS; (**b1**–**b4**) are those of RADAR; (**c1**–**c4**) are those of IMERG; (**d1**–**d4**) are those of GSMAP; (**e1**–**e4**) are those of ERA5.

3.2. Temporal Variation of Precipitation

Figure 6a displays the time series of hourly average precipitation for rain gauges and precipitation products during the "7.20" Henan rainstorm. Figure 6b illustrates the corresponding cumulative average precipitation curves over time. Throughout the entire precipitation process, CMPAS exhibits almost perfect agreement with the rain gauges in terms of regional average precipitation, with a CORR value of 0.96. Periods of heavy precipitation mainly occur between 00:00 on July 19 and 00:00 on July 22. The RADAR reflects an overestimation of precipitation throughout the entire period, particularly during periods of heavy rainfall. The IMGER and GSMAP underestimate precipitation before 00:00 on July 19, but there is a better agreement with observations after that. The ERA5, on the other hand, demonstrates better agreement with observations before 00:00 on the 19th but systematically underestimates precipitation as the intensity increases during the rainfall process. In the core precipitation area (Figure 6c,d), the findings are generally consistent with those of the entire study area, except that RADAR and IMERG exhibit a more pronounced regional overestimation of precipitation during the peak period (03:00–09:00 on the 20th), while ERA5 also demonstrates a more noticeable underestimation.

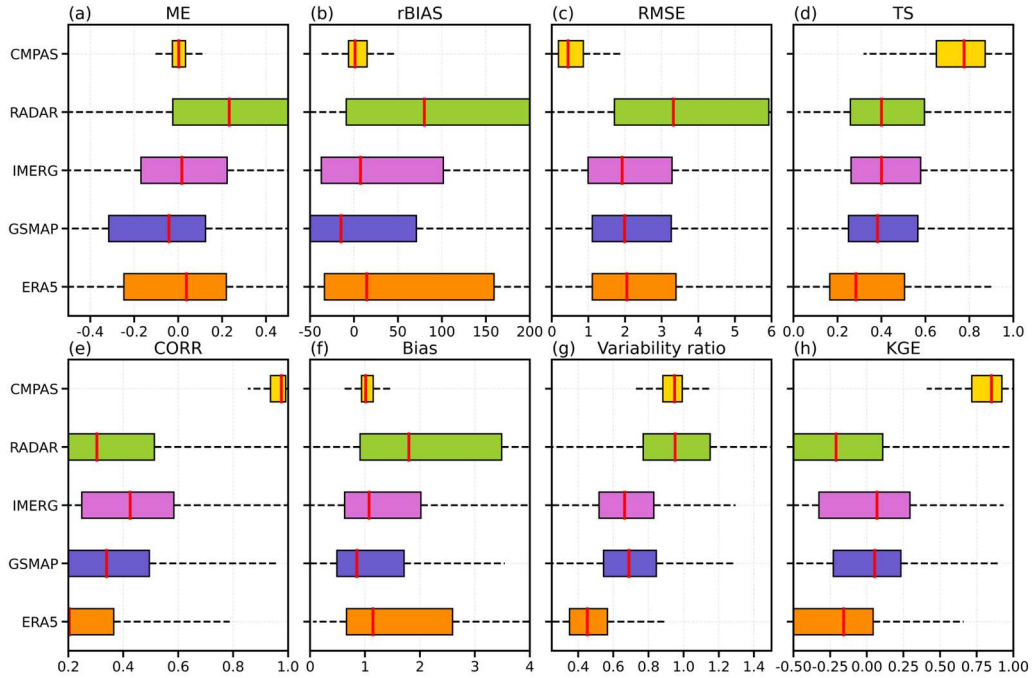

Figure 5. Boxplots of the precipitation products for various assessment metrics during the "7.20" Henan rainstorm. The red lines indicate the median; the left and right boundary lines of each box plot indicate the 25th and 75th percentile of that assessment indicator, respectively. (**a**) ME, (**b**) rBIAS, (**c**) RMSE, (**d**) TS score, (**e**) CORR, (**f**) Bias, (**g**) VAR and (**h**) KGE.

Table 1. Scoring metrics for the precipitation products during the "7.20" Henan rainstorm. The units of ME and RMSE are mm/h; the units of rBIAS are %.

	ME	rBIAS	RMSE	CORR	Bias	Var	KGE	TS
CMPAS	0.007	1.07	0.88	0.961	1.01	0.948	0.934	0.791
RADAR	0.521	77.9	5.439	0.385	1.779	1.018	0.007	0.556
IMERG	0.0002	0.031	2.867	0.486	1.0003	0.701	0.405	0.456
GSMAP	−0.144	−21.63	2.917	0.415	0.783	0.655	0.288	0.442
ERA5	−0.056	−8.425	3.105	0.278	0.915	0.476	0.104	0.341

Figure 7 shows the time series of the evaluation indicators of various precipitation products across the entire study area (left) and the core precipitation area (right) during the "7.20" Henan rainstorm. It can be observed that the evaluation indicators for CMPAS remain relatively stable over time, indicating its consistent quality compared to other precipitation products. The assessment results of CMPAS are closer to the optimal values for each indicator. The ME and RMSE values for RADAR increase significantly with precipitation, resulting in larger error values than other products, with ME exceeding 1 mm/h and RMSE reaching 8 mm/h. The ME and RMSE values of IMERG, GSMAP and ERA5 are similar, which also change consistently over time. In terms of precipitation capture ability (TS score and FBI), RADAR, IMERG, GSMAP and ERA5 exhibit consistent performance over time, with ERA5 performing slightly worse than the others at certain times. In the core precipitation area, there is a notable increase in the ME and RMSE indicators for all precipitation products due to the increase in precipitation magnitude. The TS scores for different products show a significant increase in the precipitation core area, reaching above 0.8, indicating that these products are less likely to miss strong precipitation processes in the core area compared to weak precipitation outside the core area.

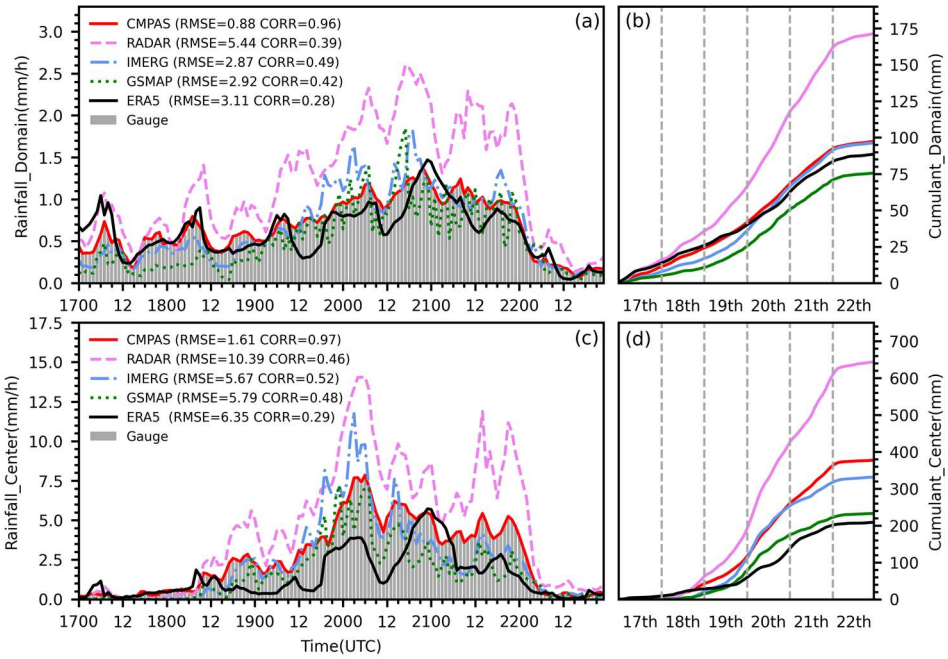

Figure 6. During the "7.20" Henan rainstorm, (**a**) shows the time series variation of regional average precipitation (unit: mm/h) of gauge observations and various precipitation products in the whole study area, (**b**) shows the time series variation curve of cumulative average precipitation (unit: mm). (**c**,**d**) are similar to (**a**,**b**) but for the core area of precipitation.

Figure 8 compares the comprehensive performance of the various precipitation products at different hourly rain intensities. It can be observed that CMPAS has the lowest RMSE and FAR, as well as the highest POD and TS scores across all rain intensity ranges compared to other products, with ME remaining mostly around 0 and FBI around 1. However, for precipitation > 20 mm/h, both ME and FBI values fall below optimum values, indicating that CMPAS becomes less effective in detecting heavy precipitation above 20 mm/h compared to other rain intensity classes. This highlights an aspect for future improvement of CMPAS. The RMSE of RADAR is significantly greater for rain intensity less than 20 mm/h, indicating that the overestimation of precipitation by RADAR is mainly concentrated in precipitation below 20 mm/h. For precipitation (>10 mm/h), the POD of RADAR is lower (<0.3), the FAR is higher (>0.7) and the FBI is abnormally high. The FBI reaches 2 for precipitation (>20 mm/h), indicating a large false area of strong precipitation detected by RADAR. The scores of the IMERG, GSMAP and ERA5 products are similar for each precipitation threshold, indicating that the three products are of comparable quality, with FAR > 0.4, TS scores < 0.5 and POD > 0.6 for precipitation < 2 mm/h.

3.3. Probabilistic Statistics of the Occurrence of Precipitation

The probability density distribution (PDF) of hourly precipitation during the rainstorm (Figure 9) shows overall good agreement between various precipitation products and gauges. There are two extreme values, with the largest one (precipitation in the range of 0.1–0.25 mm/h) accounting for about 28% and precipitation in the range of 1–2.5 mm/h accounting for about 18%, while the maximum hourly precipitation exceeds 200 mm/h. The PDF of precipitation in the range of 0.1–0.25 mm/h for CMPAS is 8% lower than that for rain gauges but 5% higher than that for rain gauges in the range of 0.25 to 0.5 mm/h. The PDF of RADAR is also close to gauges, but there is a relative overestimation of precipitation in the range of 7.5–50 mm/h. The IMERG and GSMAP significantly overestimates precipitation at the second peak, with GSMAP overestimating by 8%, but underestimates precipitation in the range of 7.5–50 mm/h. The ERA5 is closest to gauges for PDF in the range of 0.1–0.25 mm/h, with greater deviations in other ranges. In general, there is a similarity

between PDFs obtained from both precipitation products and rain gauge observations, but PDFs for precipitation products in the range of 0.1–0.25 mm/h are low, whereas the estimates for the range of 0.25–2.5 mm/h are high.

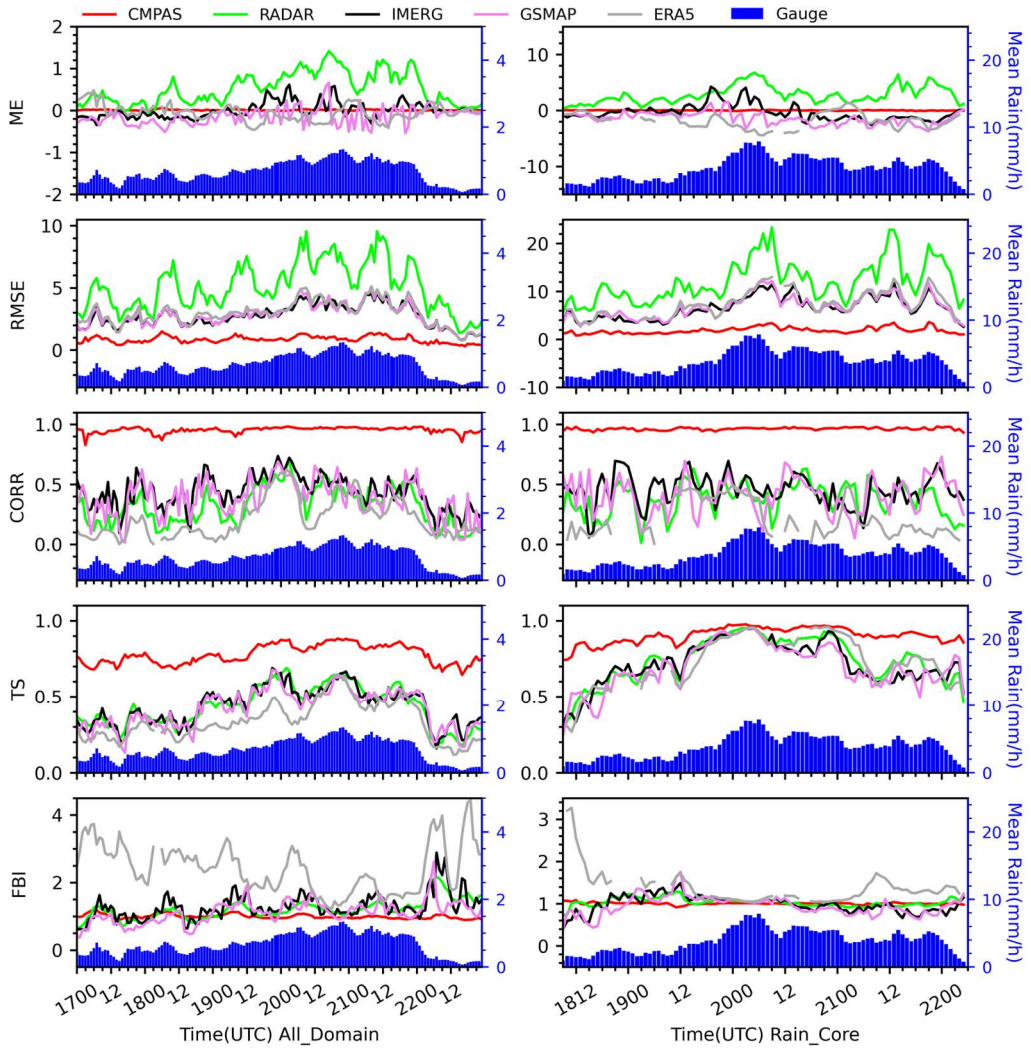

Figure 7. Time series of the evaluation indicators (curve) for the various precipitation products and mean gauges precipitation (bar) in the whole study area (**left**) and the core area of precipitation (**right**) during the "7.20" Henan rainstorm. From top to bottom: ME, RMSE, CORR, the TS score and FBI.

The sensitivity of various precipitation products to the detection of rainfall events can be revealed by further analysis of the cumulative distribution function [54] in terms of coincidence (CDFc) and volume (CDFv). Figure 10a shows that, except for ERA5, all precipitation products have a CDFc similar to that of rain gauges. For precipitation < 1.5 mm/h, CMPAS has a lower CDFc compared to gauge observations, but they are similar for precipitation > 2 mm/h, indicating that CMPAS is biased in capturing small precipitation but consistent with gauges for higher amounts (>1.5 mm/h). The RADAR's CDFc curve lies below gauge observations and is the last product to reach 100% CDFc, suggesting that RADAR detects more spurious heavy precipitation. The IMERG and GSMAP both have similar CDFc values, which are lower than rain gauges for precipitation < 2 mm/h and much higher than the rain gauges for precipitation > 2 mm/h, indicating both products are inadequate at detecting light precipitation events (<2 mm/h) and better at detecting precipitation events of 2–8 mm/h. The CDFc curve for ERA5 lies entirely above rain gauge observations and reaches 100% at the fastest rate, indicating that ERA5 is least effective at detecting heavy precipitation.

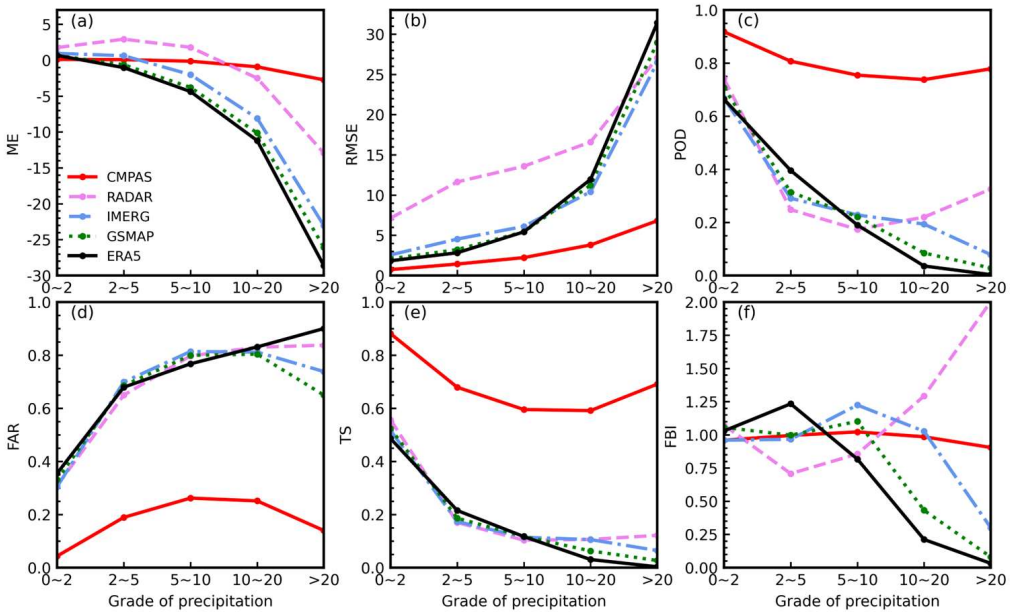

Figure 8. Statistics of the evaluation results for the precipitation products at different hourly precipitation threshold intervals during the "7.20" Henan rainstorm. (**a**) ME, (**b**) RMSE, (**c**) POD, (**d**) FAR, (**e**) FBI and (**f**) TS score.

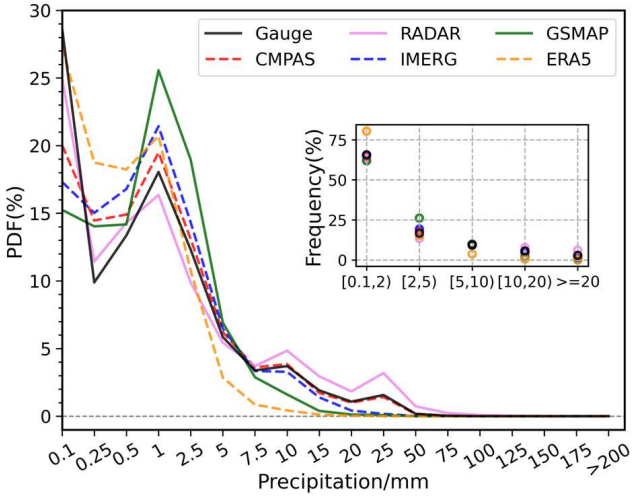

Figure 9. Probability density function (PDF, unit: %) curves of the hourly precipitation for gauge observations and precipitation products during the "7.20" Henan rainstorm, with subplots showing the frequency (unit: %) of occurrence of different hourly rain intensities.

For the CDFv, CMPAS gives similar results to the rain gauges, except for a slightly higher CDFv between 2 and 24 mm/h. The CDFv curve of RADAR is located at the right of observations, indicating that RADAR contributes the most to the total precipitation volume through strong precipitation. The curves of IMERG, GSMAP and ERA5 are located at the left of observations, indicating that these three precipitation products contribute the most to the total precipitation volume through weak precipitation. Specifically, hourly precipitation ranging from 0 to 4 mm/h in ERA5 contributes 60% of the total precipitation. Figure 10c,d display CDF curves of the RMSE and correlation coefficient for each type of precipitation product. In terms of error distribution, CMPAS have the minimal RMSE and highest correlation coefficient values among all products evaluated. The CDF curves of RMSE for IMERG, GSMAP and ERA5 are identical and superior compared to RADAR's curve. The order of correlation coefficients is as follows: CMPAS > IMERG > GSMAP and RADAR > ERA5.

The structure of the spatial distribution (Figure 11b) of the maximum hourly rainfall intensity and the PDF of the maximum hourly rainfall intensity (Figure 11a) for each precipitation product throughout the rainstorm are presented in Figure 11. The gauge observations indicate that the maximum hourly rain intensity during this process is mainly concentrated between 10 mm/h and 31.6 mm/h. Among all precipitation products, CMPAS has a PDF distribution shape closest to that observed by gauges. The maximum hourly rainfall intensity for RADAR is concentrated between 10 and 100 mm/h, with the PDF peak occurring at precipitation of 31.6 mm/h, which exceeds the results from gauges. The distribution of maximum hourly rain intensity for IMERG, GSMAP and ERA5 is significantly smaller compared to gauges, with the peak precipitation of PDF also being smaller than that observed by gauges, further illustrating the apparent underestimation of precipitation. The structure of the spatial distribution of the maximum hourly rainfall intensity is essentially similar to that of gauge observations. However, because CMPAS is a grid product with a higher spatial resolution, it can represent more precipitation details than gauge observations. The RADAR significantly overestimates maximum hourly precipitation in the core precipitation area, with large areas of greater than 200 mm/h rainfall intensity. At the periphery of the core, RADAR still agrees well with observations. The IMERG captures precipitation distributions exceeding 50 mm/h, while both GSMAP and ERA5 reflect maximum hourly precipitation less than 50 mm/h. The reason why satellite products are weak in capturing this extreme precipitation is that IMERG and GSMAP heavily rely on the scattering signal of ice phase particles within rain clouds when using the QPE algorithm to retrieve land precipitation based on PMW. When there are no or few ice particles in the topographic cloud, the estimation of extreme precipitation is less accurate than expected [55]. As for ERA5, the precipitation in the reanalysis is generally forecast by the model; however, its sub-grid convection parameterization schemes have limitations that can not reveal the convective activity effectively, resulting in poor monitoring performance for heavy precipitation, especially convective rainfall [56,57].

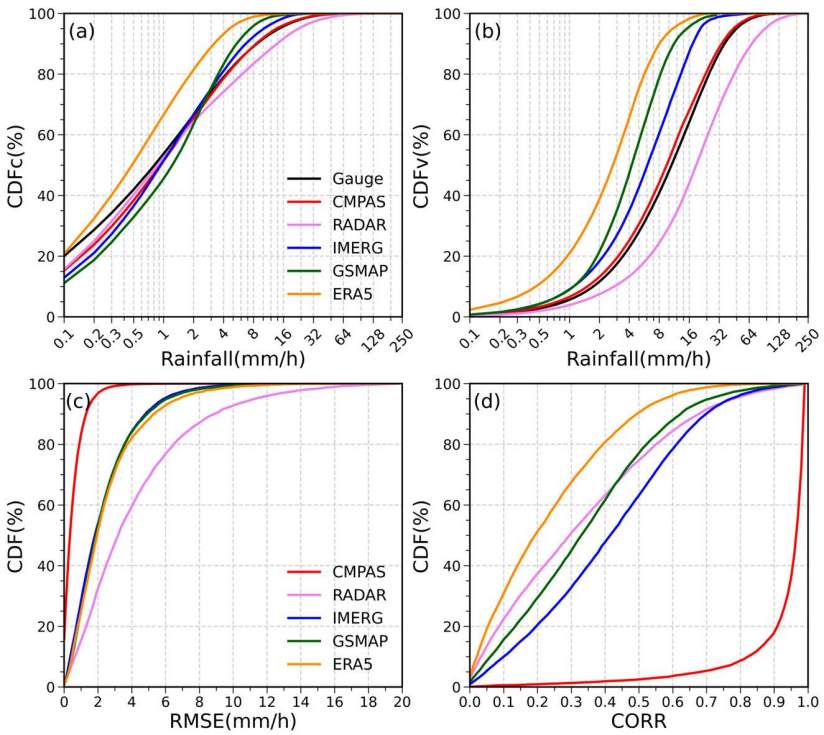

Figure 10. (**a**) Cumulative distribution of rainfall rates for gauges and various precipitation products in terms of occurrence (CDFc) and (**b**) volume (CDFv). The interval used here is 0.1 mm/h. (**c**) The cumulative distribution function curves of the RMSE of precipitation products and (**d**) the cumulative distribution function curve of CORR of the precipitation products.

3.4. Daily Variation of Precipitation

Figure 12 illustrates the longitudinal representation of the average daily variation in hourly precipitation for each product. The precipitation products consistently indicate that this precipitation event lacks significant eastward propagation characteristics, instead primarily occurring within the range of 112.5°E to 115°E, with two extreme centers of precipitation near 03:00 and 12:00. The daily precipitation variation characteristic of CMPAS is most similar to gauge observations. There is a positive precipitation deviation exceeding 1.6 mm/h in RADAR between 00:00 and 18:00. The precipitation distribution structure of IMERG is basically consistent with observations, but there is a two-hour delay in the peak precipitation and a shift of the extreme center toward the east. The GSMAP only shows unimodal distribution as an estimated center for precipitation extremes, with an overall eastern shift of precipitation. The daily precipitation patterns of ERA5 exhibit inconsistencies with observations, and the primary rain belt extends toward the west. Figure 12c shows the daily variation in mean precipitation across the entire study area, indicating that all other precipitation products are similar to gauge observations except for RADAR, which systematically appears stronger.

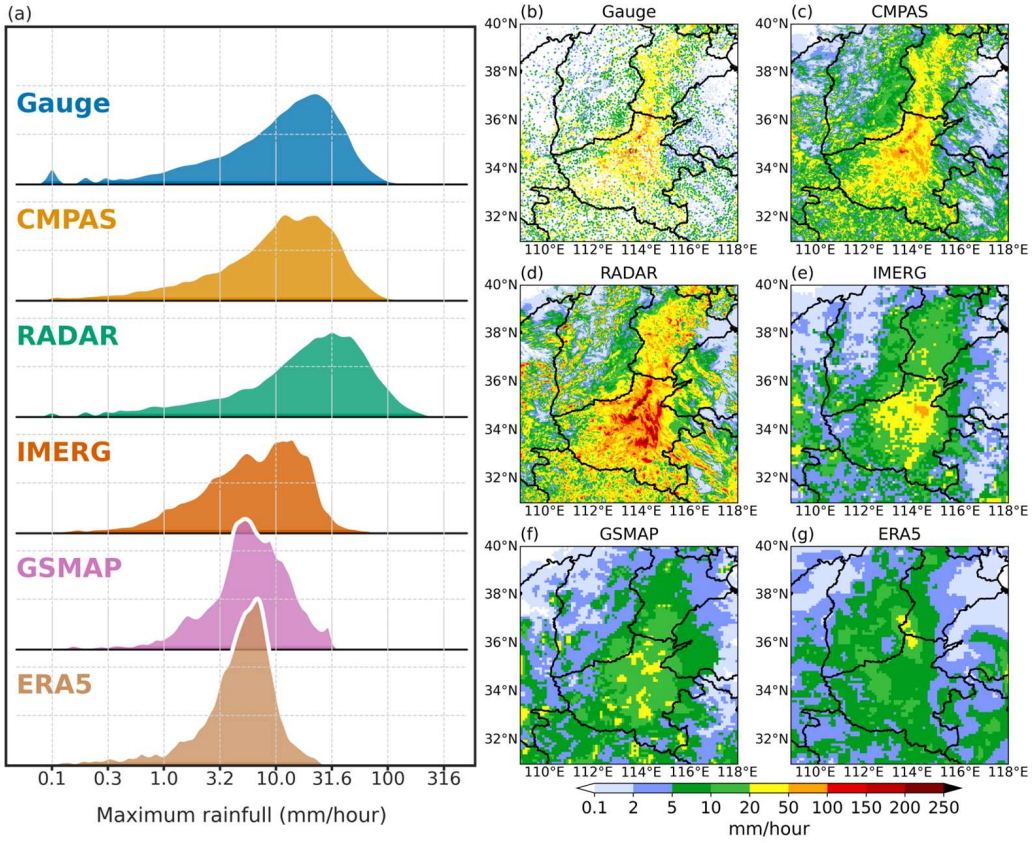

Figure 11. (**a**) Probability density function (PDF, unit: %) plots of maximum hourly rainfall from gauges and various precipitation products during the "7.20" Henan rainstorm. (**b**–**g**) Spatial distribution of the maximum hourly rainfall (unit: mm/h) from gauges and various precipitation products at the original resolution, in the order of gauges, CMPAS, RADAR, IMERG, GSMAP, ERA5.

To investigate whether deviations in daily variability are related to precipitation intensity classes, we further calculate the joint probability density distribution function (JPDF) of rain intensity and day variability [58]. Across the entire study area (Figure 13), rain gauges show obvious daily variation in the different precipitation classes. Precipitation is primarily concentrated during the day and after midnight, with weaker precipitation between 10:00 and 15:00 (UTC). The higher the rainfall intensity, the greater its contribution to the total precipitation, especially for rainfall exceeding 20 mm/h. The peak time for

precipitation occurs from 06:00 to 08:00 (UTC). The CMPAS reflects the same pattern with gauges but has a lower contribution of precipitation during peak time for heavy rainstorms (>20 mm/h). The RADAR significantly overestimates heavy rainstorms while underestimating moderate-intensity precipitation; however, the daily variability pattern is consistent with gauges. The IMERG, GSMAP and ERA5 exhibit obviously high contributions to the total precipitation within the rainfall intensity range below 10 mm/h.

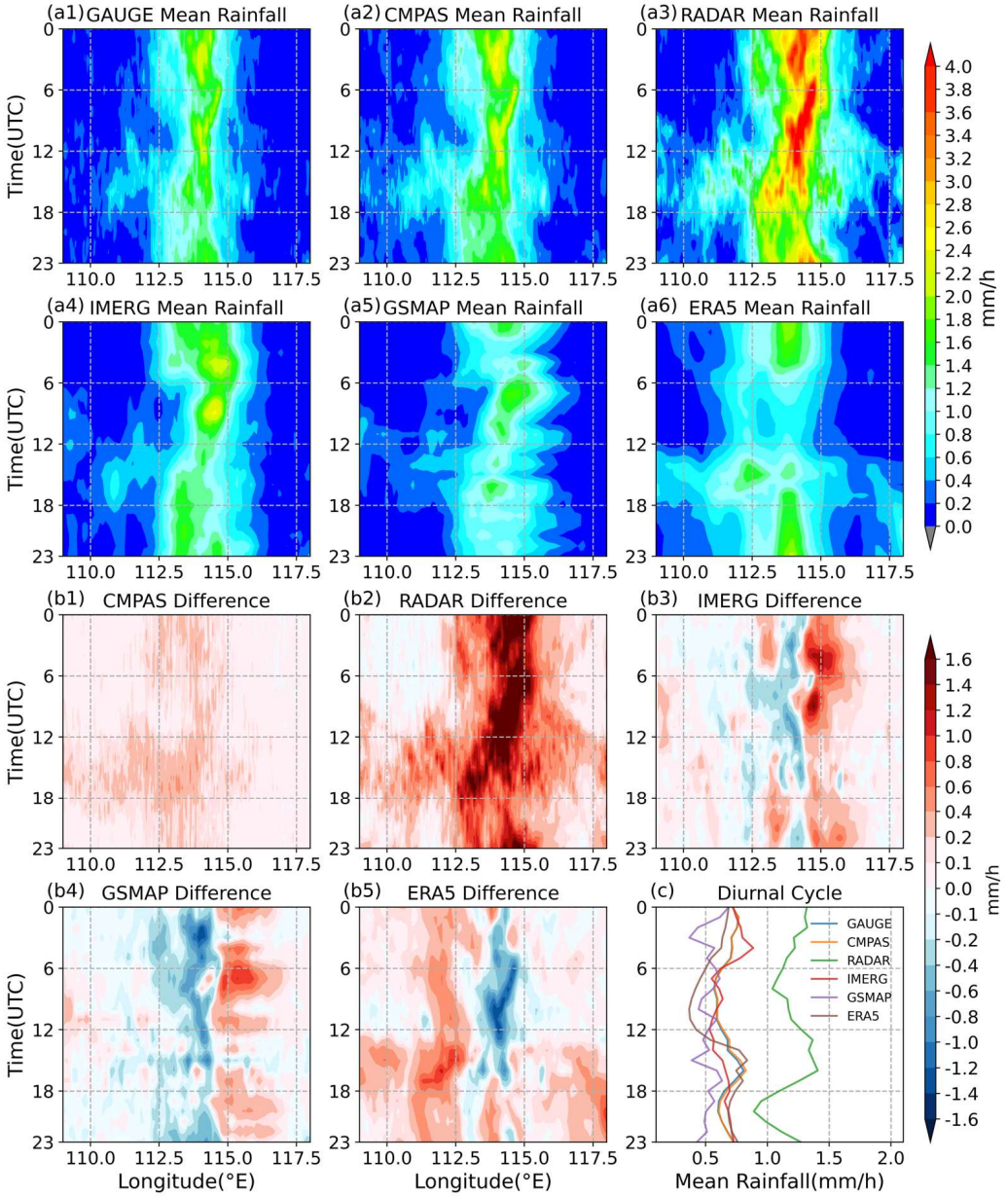

Figure 12. (**a1**–**a6**) The meridional daily variation of mean hourly rainfall (unit: mm/h) from gauges and precipitation products during the "7.20" Henan rainstorm (17–22 July 2021). (**b1**–**b5**) Daily variation difference between precipitation products and gauges. (**c**) The daily variation in average precipitation (unit: mm/h) across the whole study area.

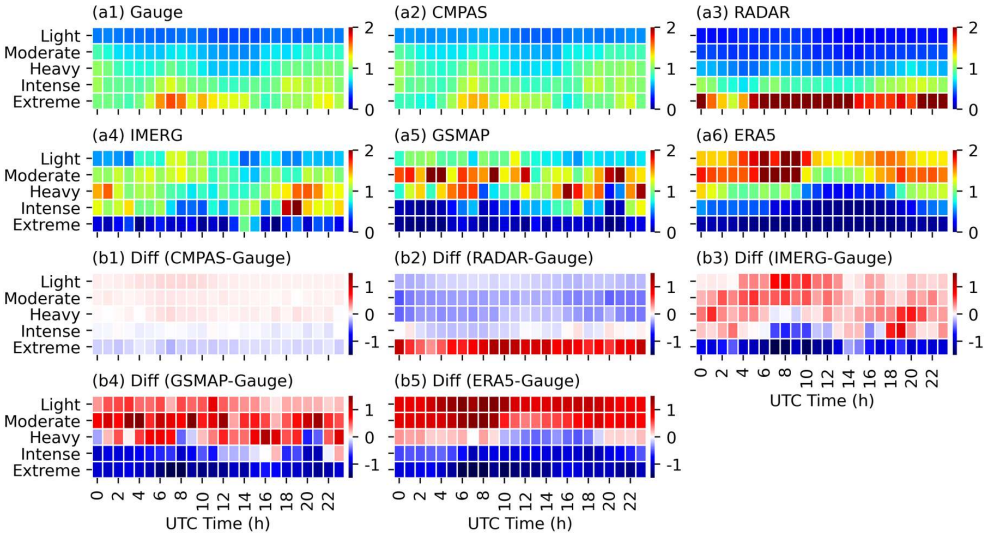

Figure 13. Comparative analysis of the daily variation of the joint probability density function (JPDF) between gauges (**a1**) and precipitation products (**a2**–**a6**) by rain intensity class during "7.20" Henan rainstorm, and the JPDF difference between the precipitation products and gauges (Diff = precipitation products − gauges; (**b1**–**b5**)).

4. Discussion

The "7.20" Henan rainstorm event is characterized by its long duration, heavy hourly rainfall intensity, large cumulative rainfall and wide coverage, causing significant damage throughout the region. High-resolution precipitation estimation products have broad applications in scientific research and operations, such as the initial field of model forecasting, meteorological disaster monitoring and warning, simulation of catastrophic flash floods and numerical model evaluation. In this study, we fully understand the performance of CMPAS, RADAR, IMERG, GSMAP and ERA5 in monitoring extreme rainfall in the Henan region by analyzing the spatiotemporal distribution of precipitation errors, probability statistics of precipitation occurrence and diurnal variability characteristics of precipitation. Overall, the CMPAS has the best evaluation indicators compared to other products in the monitoring of the "7.20" Henan rainstorm with 0.88 mm/h (RMSE), 1.07% (rBIAS), 0.961 (CORR), 0.791 (TS) and 0.934 (KGE). The CMPAS exhibits a remarkable resemblance to rain gauges in accurately capturing the intricate characteristics of regions with heavy rainfall, representing the intensity distribution of precipitation centers and depicting the temporal evolution features of precipitation systems. With a spatial resolution of $0.01^\circ \times 0.01^\circ$, CMPAS effectively complements precipitation information in areas where station observations are lacking.

Typically, a sufficient number of samples is employed to demonstrate the statistical significance of the results. Therefore, in order to further validate the reliability and applicability of the aforementioned conclusions and minimize misjudgments regarding precipitation product performance, we have supplemented three instances of catastrophic rainfall that occurred in July 2022 for comparative analysis. The time periods during which these three heavy rain events took place are as follows: Case 1 (3–6 July 2022), Case 2 (22–23 July 2022) and Case 3 (25–28 July 2022).

The "7.20" Henan rainstorm event, which occurs once every few decades, is an exceptional occurrence. Although the three selected instances of heavy rainfall can not reach the same unprecedented intensity as the "7.20" Henan rainstorm, they still result in a certain degree of economic loss. The results presented in Figure 14 demonstrate that five precipitation products can successfully capture the occurrence of these three intense rainfall events. A comparison with gauge observation reveals that CMPAS exhibits superior performance compared to other types of precipitation products, particularly in terms of its precise spatial depiction of precipitation distribution and accurate representation of extreme values

associated with heavy rainfall centers. Specifically, in case 3, accumulated precipitation exceeding 50 mm impacts areas located in the southern part of Hebei Province as well as the central and southern parts of Henan Province. These regions exhibit a locally scattered distribution pattern, which demands high precision for accurately capturing local precipitation zones by precipitation products. The CMPAS demonstrates superior agreement with observations, while RADAR significantly overestimates the extent of precipitation, surpassing 50 mm and 100 mm. Two satellite products (IMERG and GSMAP) roughly depict these three intense rainfall regions but lack detailed characterization. The ERA5 exhibits the poorest performance.

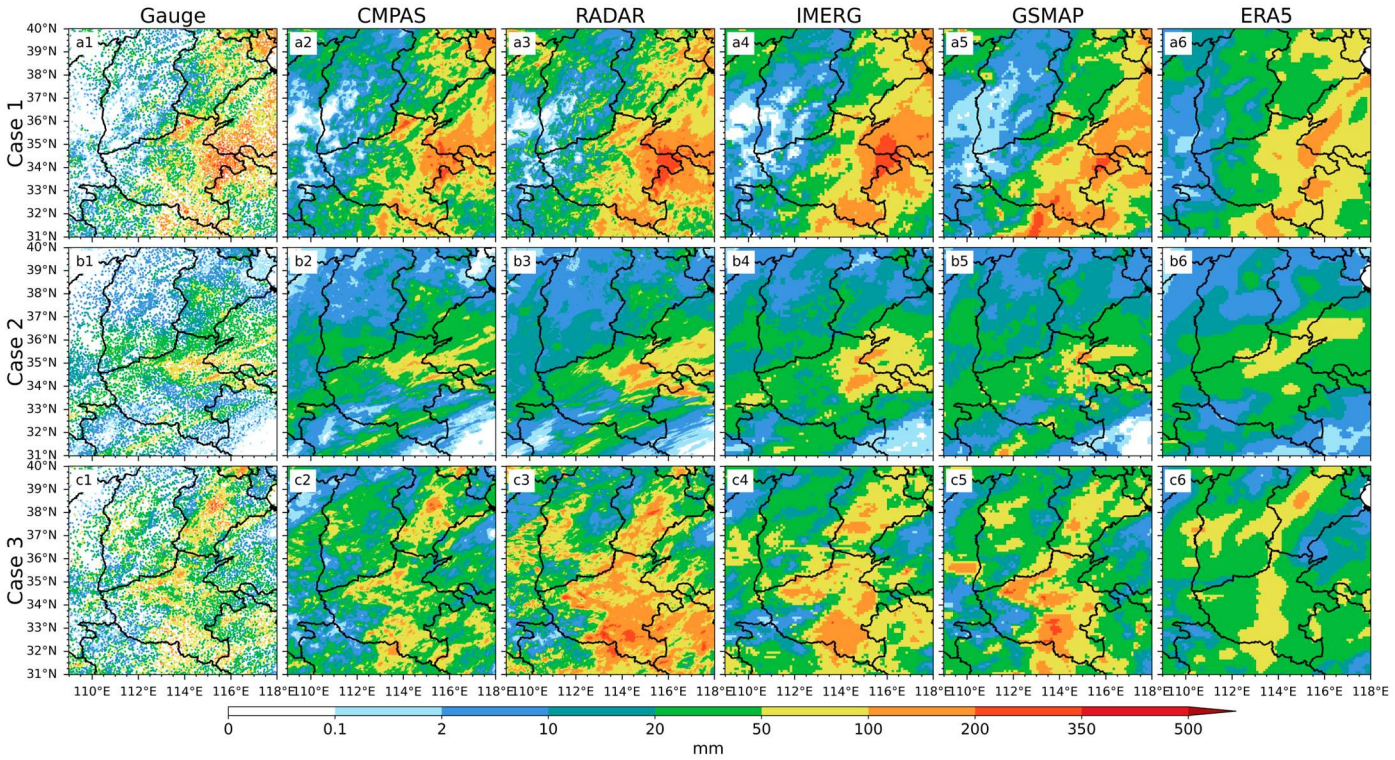

Figure 14. The spatial distribution of accumulated precipitation (unit: mm) during the three heavy rainfall cases in Henan province in July 2022. (**a1**–**a6**) represent case 1, respectively, for gauge observations, CMPAS, RADAR, IMERG, GSMAP and ERA5; (**b1**–**b6**) represent case 2; (**c1**–**c6**) represent case 3.

The differences between various precipitation products and gauge observations in terms of hourly rainfall are also compared for three cases (Figure 15). The fitting line of the CMPAS exhibited the closest proximity to the 1:1 line, although still slightly below it, indicating a persistent tendency to underestimate precipitation, especially for heavy rainfall exceeding 50 mm/h. The overall performance of RADAR, IMERG, GSMAP and ERA5 in fitting hourly rainfall intensity in three case studies is consistent with their performance during the "7.20" Henan rainstorm. The RADAR still exhibits false intense precipitation, while IMERG, GSMAP and ERA5 still fail to effectively capture rainfall exceeding 50 mm/h. Additionally, we provide box plots (Figure 16) illustrating the distribution of error metrics for various precipitation products during three case studies. The overall evaluation results of these three cases are consistent with the "7.20" Henan rainstorm. However, since these three cases are not as extreme as the "7.20" Henan rainstorm, there has been an enhancement in the detection capability for precipitation (as measured by TS scores) across all four products: RADAR, IMERG, GSMAP and ERA5.

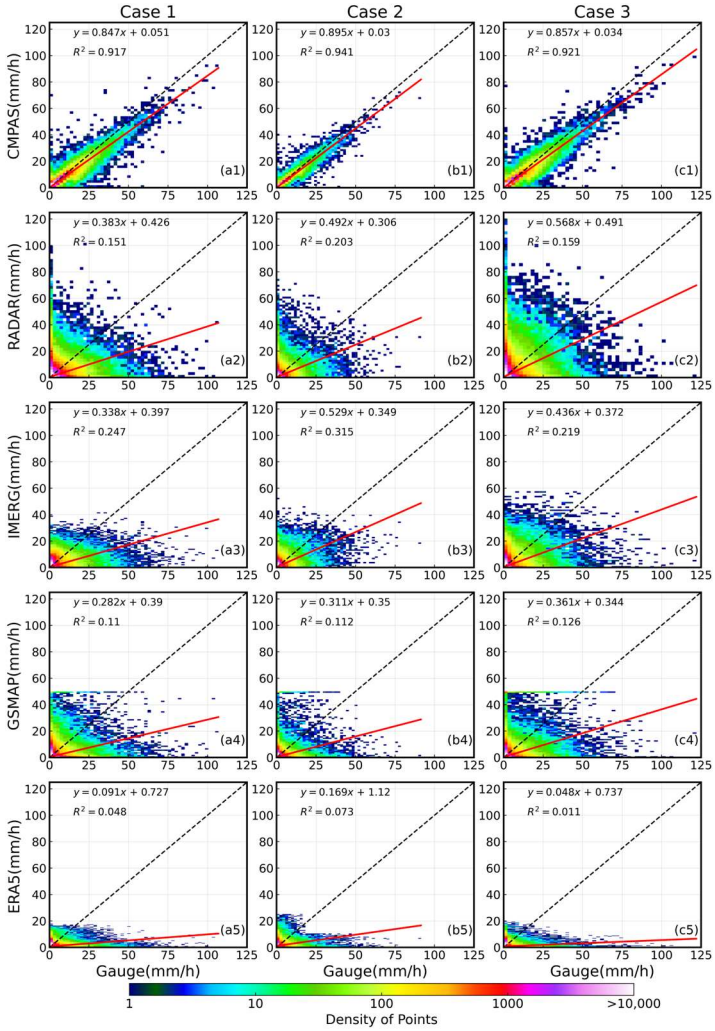

Figure 15. Scatter comparison diagram of hourly rainfall (unit: mm/h) observed by gauges and precipitation products during three cases in July 2022, as well as their linear regression distribution fitting (red line). (**a1**–**a5**) represent case 1, respectively, for CMPAS, RADAR, IMERG, GSMAP and ERA5; (**b1**–**b5**) represent case 2; (**c1**–**c5**) represent case 3.

The CMPAS represents a high degree of agreement with rain gauge observation, indicating its potential for hydrological utilization due to its 1 h/0.01° temporal and spatial resolution, which allows it to capture more precipitation details than rain gauges. However, the RADAR, IMGRG, GSMAP and ERA5 products tend to overestimate small precipitation and underestimate large precipitation in different degrees. This is due to the difference between observation systems and observation equipment and the limitation of observation technology. The observation error of data always exists objectively [20–26]. The performance of monitoring different precipitation intensities of 10 satellite precipitation products in this extreme heavy rain event studied by Liu et al. [59] showed a similar phenomenon. Prakash et al. [60] conducted a daily assessment of the GSMAP-NRT product and found that it underestimates rainfall in most parts of India. ERA5 has shown excellent application in simulating global storm surges [61]. Wu et al. [62] pointed out that there is still room for improvement in the FY-2H QPE's precipitation retrieval algorithm. Error correction algorithms are necessary, especially for rainstorm events occurring in complex topography. Li et al. [63] pointed out that CMPAS shows a high consistency with the observed data in the Sichuan Basin; however, its applicability in plateau regions still needs further research due to factors such as sparse station coverage and complex terrain. Gentilucci et al. [64] validated the IMERG product at annual and monthly scales by pixel-

to-pixel and found that it performs worse in coastal and hilly areas. Therefore, how to effectively combine the advantages of precipitation data from different sources and develop multi-source precipitation-merging technology has become the mainstream trend in the development of high-quality precipitation products in the world in recent decades [65–67]. Although CMPAS has performed very well, there are still many problems that need to be solved, such as the scientific elimination of the systematic bias of various observation data and the influence of complex underlying surface conditions, so as to obtain more accurate precipitation real data.

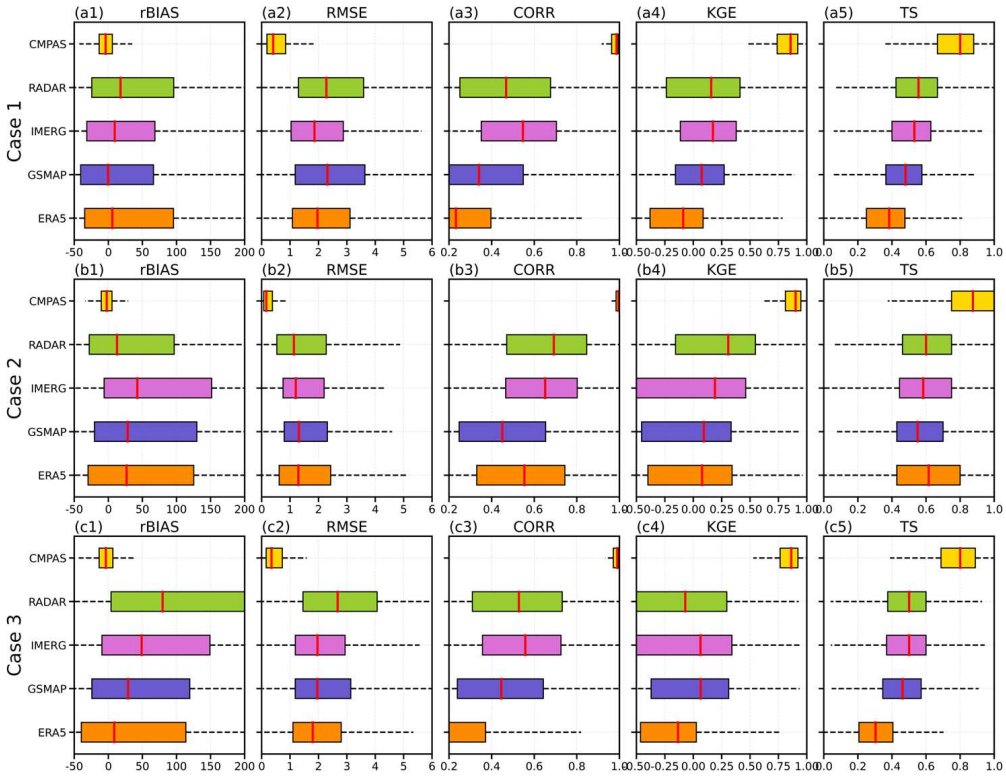

Figure 16. Boxplot of the evaluation indicators of precipitation products during three Henan cases in July 2022; the red line in the box represents the median, and the left and right boundaries of each box represent the 25th and 75th percentiles of the evaluation indicators, respectively. (**a1**–**a5**) represent case 1, respectively, for rBIAS, RMSE, CORR, KGE and TS score; (**b1**–**b5**) represent case 2; (**c1**–**c5**) represent case 3.

5. Conclusions

In this study, the extreme precipitation monitoring capability of five precipitation products is systematically investigated during the "7.20" Henan rainstorm, using dense surface rain gauge observation data for reference. The main findings are as follows:

1. Regarding the spatial characteristics of precipitation analysis, the CMPAS shows the best performance in terms of fitting with gauge observations, particularly in precipitation distribution and extreme values at the center of heavy rainfall, with rBIAS, RMSE, CORR, KGE and TS scores of 1.07%, 0.88 mm/h, 0.961, 0.934 and 0.791, respectively. The spatial variability of error in CMPAS is minimal, and the product remains regionally stable. The RADAR significantly overestimates the cumulative precipitation, primarily due to a large number of falsely estimated heavy rainfall exceeding 100 mm/h. The overall RMSE of RADAR is 5.43 mm/h, with bias mainly concentrated in the core precipitation area in central Henan Province. The IMERG, GSMAP and ERA5 exhibit similar performance, with IMERG showing slightly better error performance. There is a significant underestimation of the cumulative rainfall in the core precipitation areas, and none of IMERG, GSMAP and ERA5 can capture heavy rainfall

exceeding 60 mm/h. In the mountainous areas of northwestern Henan Province, there are negative biases in precipitation products, indicating the need for terrain error correction for satellite and model precipitation products in complex terrain.

2. Regarding the temporal characteristics of precipitation analysis, the CMPAS accurately captures the evolution of the average precipitation in the region, and all evaluation indicators are stable and better than those of other precipitation products. The RADAR significantly overestimates during peak precipitation periods in the core precipitation area, with the largest deviation values and RMSE reaching 8 mm/h. The TS scores of IMERG and GSMAP are higher during heavy rainfall periods (0.6) compared to light rainfall periods (0.4), and the TS score for the precipitation core area (0.8) is higher than that for the entire study area (0.6). The ERA5 matches well and initially gauges moderate-intensity rainfall but then significantly underestimates after heavy rainfall begins, particularly in the core precipitation area where underestimation is more pronounced. In terms of the precipitation grading test, the CMPAS has slightly lower ME and FBI scores than the optimal values for rainfall exceeding 20 mm/h, indicating an underestimation of heavy rainfall estimation. The RADAR has a significantly higher RMSE in precipitation intensity below 20 mm/h, indicating that RADAR mainly produces false overestimation for small to large rainfall. The scores of IMERG, GSMAP and ERA5 are better for light rainfall compared to heavy rainfall.
3. In terms of the probability statistical characteristics of precipitation occurrence, various precipitation products exhibit a similar PDF distribution to rain gauge observations when estimating hourly rainfall intensity. However, there is an underestimation in the probability estimation of precipitation occurrence in the range of 0.1–0.25 mm/h, while overestimation occurs in the range of 0.25–2.5 mm/h. When the hourly rainfall intensity exceeds 7.5 mm/h, the CMPAS and rain gauges show complete consistency in their PDFs, while RADAR overestimates and IMERG, GSMAP and ERA5 underestimate it. In ERA5, an hourly precipitation intensity of 0–4 mm/h contributes 60% of the total precipitation, while gauges and CMPAS are mainly concentrated in the range of 2–24 mm/h. The analysis of hourly maximum rainfall intensity of various precipitation products further indicates the consistency between CMPAS and rain gauge observations, the overestimation of precipitation by RADAR and the weak ability of IMERG, GSMAP and ERA5 products to capture the extreme values of heavy rainfall.
4. In terms of the diurnal variation characteristics of precipitation, there is no obvious east–west propagation of precipitation in this precipitation process. Instead, it mainly occurs between 112.5 and 115°E, with two precipitation peak centers near 03:00 and 12:00. Both rain gauges and CMPAS reflect that the contribution rate of rainfall intensity to total precipitation is positively correlated. However, the CMPAS underestimates the extremely heavy rainfall during the peak period (06:00–08:00). Precipitation greater than 20 mm/h in the RADAR makes the largest contribution to total precipitation and is significantly overestimated from 08:00 to 14:00. The precipitation peak time estimated by IMERG lags by 2 hours. The GSMAP only reflects a single-peak structure of precipitation, while ERA5 has a diurnal variation structure opposite to gauge observations. Throughout the day, the IMERG, GSMAP and ERA5 generally overestimate rainfall from light to heavy levels but underestimate the contribution of rainstorms and heavy rainstorms to total precipitation.

Our study provides a comprehensive evaluation of the precipitation characteristics, error indicators and diurnal variation rules of radar precipitation estimation product (RADAR), satellite precipitation products (IMERG, GSMAP), reanalysis product (ERA5),and multi-source observation precipitation fusion product (CMPAS) during the "7.20" Henan rainstorm period. Additionally, we conduct further discussions on three other precipitation cases occurring in the Henan region to analyze the applicability of the methods used in a series of events and compare the consistency of results from these three cases with those of the '7.20' Henan rainstorm. However, in order to gain a deeper understanding of the root causes of the errors, further work will be needed in the future. This being the case,

it is necessary to further consider the influence of different terrain factors on the comprehensive performance of precipitation products, as well as research on correction methods for extremely heavy rainfall events, and analyze the applicability of different precipitation products in driving hydrological models to simulate flash flood processes.

Author Contributions: Z.P. and C.S. conceived and designed the experiments; Z.P. and Y.Z. performed the experiments, analyzed the data and wrote the original version; J.G., Q.Y., Y.P., Z.W. and B.X. polished the document. All authors have read and agreed to the published version of the manuscript.

Funding: This research was funded by the National Science Foundation of China (Grant No. 42205049), Advance Research on Civil Space Technology During the 14th Five-Year Plan (Grant No. D040405), Special fund of China Meteorological Administration Rainstorm Fine Analysis and Forecast Youth Innovation Team (Grant No. CMA2023QN05), Scientific and Technological Innovation Platform of Global Atmospheric Background and Tibetan Plateau Big Data Application Center (Grant No. 2023-SF-J10) and the Satellite Application Advance Plan of Feng-Yun (Grant No. FY-APP-2022.0608).

Data Availability Statement: The CMPAS, RADAR product and gauge observations data are freely available at http://data.cma.cn/en. The IMERG product data are freely available at https://disc.gsfc.nasa.gov/datasets/ (accessed on 29 October 2023). The GSMAP product data are freely available at https://sharaku.eorc.jaxa.jp/GSMaP/ (accessed on 29 October 2023). The ERA5 product data are freely available at https://cds.climate.copernicus.eu/#!/home (accessed on 29 October 2023). The datasets used and analyzed during the current study are available from the corresponding author upon reasonable request.

Acknowledgments: We thank the provider of the CMPAS, RADAR, IMGRG, GSMAP and ERA5 product and gauge observation data.

Conflicts of Interest: The authors declare no conflict of interest.

References

1. Tapiador, F.J.; Turk, F.J.; Petersen, W.; Hou, A.Y.; García-Ortega, E.; Machado, L.A.T.; Angelis, C.F.; Salio, P.; Kidd, C.; Huffman, G.J.; et al. Global precipitation measurement: Methods, datasets and applications. *Atmos. Res.* **2012**, *104–105*, 70–97. [CrossRef]
2. Tian, F.; Hou, S.; Yang, L.; Hu, H.; Hou, A. How Does the Evaluation of the GPM IMERG Rainfall Product Depend on Gauge Density and Rainfall Intensity? *J. Hydrometeorol.* **2018**, *19*, 339–349. [CrossRef]
3. Wang, X.; Ding, Y.; Zhao, C.; Wang, J. Similarities and improvements of GPM IMERG upon TRMM 3B42 precipitation product under complex topographic and climatic conditions over Hexi region, Northeastern Tibetan Plateau. *Atmos. Res.* **2019**, *218*, 347–363. [CrossRef]
4. Sharifi, E.; Steinacker, R.; Saghafian, B. Multi time-scale evaluation of high-resolution satellite-based precipitation products over northeast of Austria. *Atmos. Res.* **2018**, *206*, 46–63. [CrossRef]
5. Wang, B.; Zhang, M.; Wei, J.; Wang, S.; Li, X.; Li, S.; Zhao, A.; Li, X.; Fan, J. Changes in extreme precipitation over Northeast China, 1960–2011. *Quat. Int.* **2013**, *298*, 177–186. [CrossRef]
6. Liu, R.; Liu, S.C.; Cicerone, R.J.; Shiu, C.-J.; Li, J.; Wang, J.; Zhang, Y. Trends of extreme precipitation in eastern China and their possible causes. *Adv. Atmos. Sci.* **2015**, *32*, 1027–1037. [CrossRef]
7. Wang, X.; Jiang, W.; Wu, J.; Hou, P.; Dai, Z.; Rao, P.; Ling, Z.; Deng, Y. Extreme hourly precipitation characteristics of Mainland China from 1980 to 2019. *Int. J. Climatol.* **2023**, *43*, 2989–3004. [CrossRef]
8. Liu, M.; Xu, X.; Sun, A.Y.; Wang, K.; Liu, W.; Zhang, X. Is southwestern China experiencing more frequent precipitation extremes? *Environ. Res. Lett.* **2014**, *9*, 064002. [CrossRef]
9. Yin, J.; Gu, H.; Liang, X.; Yu, M.; Sun, J.; Xie, Y.; Li, F.; Wu, C. A Possible Dynamic Mechanism for Rapid Production of the Extreme Hourly Rainfall in Zhengzhou City on 20 July 2021. *J. Meteorol. Res.* **2022**, *36*, 6–25. [CrossRef]
10. Luo, Y.; Du, Y. The Roles of Low-level Jets in "21·7" Henan Extremely Persistent Heavy Rainfall Event. *Adv. Atmos. Sci.* **2023**, *40*, 350–373. [CrossRef]
11. Nie, Y.; Sun, J. Moisture Sources and Transport for Extreme Precipitation Over Henan in July 2021. *Geophys. Res. Lett.* **2022**, *49*, e2021GL097446. [CrossRef]
12. Zhang, G.; Mao, J.; Hua, W.; Wu, X.; Sun, R.; Yan, Z.; Liu, Y.; Wu, G. Synergistic Effect of the Planetary-scale Disturbance, Typhoon and Meso-β-scale Convective Vortex on the Extremely Intense Rainstorm on 20 July 2021 in Zhengzhou. *Adv. Atmos. Sci.* **2023**, *40*, 428–446. [CrossRef]
13. Li, Z.; Yun, C.; Zhang, F.; Sun, J.; Wang, Y.; Fu, J.; Chao, Y. Consideration by "75·8" Extreme Heavy Rainfall Event in Henan. *Meteorol. Environ. Sci.* **2015**, *38*, 1–12.

14. Villarini, G.; Krajewski, W.F.; Ciach, G.J.; Zimmerman, D.L. Product-error-driven generator of probable rainfall conditioned on WSR-88D precipitation estimates. *Water Resour. Res.* **2009**, *45*, W01404. [CrossRef]
15. Vila, D.A.; de Goncalves, L.G.G.; Toll, D.L.; Rozante, J.R. Statistical Evaluation of Combined Daily Gauge Observations and Rainfall Satellite Estimates over Continental South America. *J. Hydrometeorol.* **2009**, *10*, 533–543. [CrossRef]
16. Hong, Y.; Tang, G.; Ma, Y.; Huang, Q.; Han, Z.; Zeng, Z.; Yang, Y.; Wang, C.; Guo, X. Remote Sensing Precipitation: Sensors, Retrievals, Validations, and Applications. In *Observation and Measurement of Ecohydrological Processes*; Springer: Cham, Switzerland, 2019; pp. 107–128.
17. Collier, C.G.; Larke, P.R.; May, B.R. A weather radar correction procedure for real-time estimation of surface rainfall. *Q. J. R. Meteorol. Soc.* **1983**, *109*, 589–608.
18. Ninomiya, K.; Akiyama, T. Objective Analysis of Heavy Rainfalls Based on Radar and Gauge Measurements. *J. Meteorol. Soc. Jpn.* **1978**, *Ser II 56*, 206–210. [CrossRef]
19. Zhong, L.; Yang, R.; Chen, L.; Wen, Y.; Li, R.; Tang, G.; Hong, Y. Combined Space and Ground Radars for Improving Quantitative Precipitation Estimations in the Eastern Downstream Region of the Tibetan Plateau. Part I: Variability in the Vertical Structure of Precipitation in ChuanYu Analyzed from Long-Term Spaceborne Observations by TRMM PR. *J. Appl. Meteorol. Climatol.* **2017**, *56*, 2259–2274.
20. Wen, Y.; Cao, Q.; Kirstetter, P.-E.; Hong, Y.; Gourley, J.J.; Zhang, J.; Zhang, G.; Yong, B. Incorporating NASA Spaceborne Radar Data into NOAA National Mosaic QPE System for Improved Precipitation Measurement: A Physically Based VPR Identification and Enhancement Method. *J. Hydrometeorol.* **2013**, *14*, 1293–1307. [CrossRef]
21. Yong, B.; Ren, L.; Hong, Y.; Gourley, J.J.; Tian, Y.; Huffman, G.J.; Chen, X.; Wang, W.; Wen, Y. First evaluation of the climatological calibration algorithm in the real- time TMPA precipitation estimates over two basins at high and low latitudes. *Water Resour. Res.* **2013**, *49*, 2461–2472. [CrossRef]
22. Lu, X.; Wei, M.; Tang, G.; Zhang, Y. Evaluation and correction of the TRMM 3B43V7 and GPM 3IMERGM satellite precipitation products by use of ground-based data over Xinjiang, China. *Environ. Earth Sci.* **2018**, *77*, 209. [CrossRef]
23. Tang, G.; Ma, Y.; Long, D.; Zhong, L.; Hong, Y. Evaluation of GPM Day-1 IMERG and TMPA Version-7 legacy products over Mainland China at multiple spatiotemporal scales. *J. Hydrol.* **2016**, *533*, 152–167. [CrossRef]
24. Albergel, C.; Dutra, E.; Munier, S.; Calvet, J.-C.; Muñoz Sabater, J.; Rosnay, P.; Balsamo, G. ERA-5 and ERA-Interim driven ISBA land surface model simulations: Which one performs better? *Hydrol. Earth Syst. Sci.* **2018**, *22*, 3515–3532. [CrossRef]
25. Hersbach, H.; Bell, B.; Berrisford, P.; Hirahara, S.; Horanyi, A.; Munoz-Sabater, J.; Nicolas, J.; Peubey, C.; Radu, R.; Schepers, D.; et al. The ERA5 global reanalysis. *Q. J. R. Meteorol. Soc.* **2020**, *146*, 1999–2049. [CrossRef]
26. Wang, C.; Graham, R.M.; Wang, K.; Gerland, S.; Granskog, M.A. Comparison of ERA5 and ERA-Interim near-surface air temperature, snowfall and precipitation over Arctic sea ice: Effects on sea ice thermodynamics and evolution. *Cryosphere* **2019**, *13*, 1661–1679. [CrossRef]
27. Xie, P.; Arkin, P.A. Global Precipitation: A 17-Year Monthly Analysis Based on Gauge Observations, Satellite Estimates, and Numerical Model Outputs. *Bull. Am. Meteorol. Soc.* **1997**, *78*, 2539–2558. [CrossRef]
28. Zhang, J.; Howard, K.; Langston, C.; Kaney, B.; Qi, Y.; Tang, L.; Grams, H.; Wang, Y.; Cocks, S.; Martinaitis, S.; et al. Multi-Radar Multi-Sensor (MRMS) quantitative precipitation estimation: Initial operating capabilities. *Bull. Am. Meteorol. Soc.* **2016**, *97*, 621–637. [CrossRef]
29. Pan, Y.; Gu, J.; Yu, J.; Shen, Y.; Shi, C.; Zhou, Z. Test of merging methods for multi-source observed precipitation products at high resolution over China. *Acta Meteorol. Sin.* **2018**, *76*, 755–766.
30. Shen, Y.; Hong, Z.; Pan, Y.; Yu, J.; Maguire, L. China's 1 km Merged Gauge, Radar and Satellite Experimental Precipitation Dataset. *Remote Sens.* **2018**, *10*, 264. [CrossRef]
31. Shen, Y.; Xiong, A.; Hong, Y.; Yu, J.; Pan, Y.; Chen, Z.; Saharia, M. Uncertainty analysis of five satellite-based precipitation products and evaluation of three optimally merged multi-algorithm products over the Tibetan Plateau. *Int. J. Remote Sens.* **2014**, *35*, 6843–6858. [CrossRef]
32. Pang, Z.; Shi, C.; Gu, J.; Pan, Y.; Xu, B. Assessment of a Gauge-Radar-Satellite Merged Hourly Precipitation Product for Accurately Monitoring the Characteristics of the Super-Strong Meiyu Precipitation over the Yangtze River Basin in 2020. *Remote Sens.* **2021**, *13*, 3850. [CrossRef]
33. Zhang, A.; Xiao, L.; Min, C.; Chen, S.; Kulie, M.; Huang, C.; Liang, Z. Evaluation of latest GPM-Era high-resolution satellite precipitation products during the May 2017 Guangdong extreme rainfall event. *Atmos. Res.* **2019**, *216*, 76–85. [CrossRef]
34. Fang, J.; Yang, W.; Luan, Y.; Du, J.; Lin, A.; Zhao, L. Evaluation of the TRMM 3B42 and GPM IMERG products for extreme precipitation analysis over China. *Atmos. Res.* **2019**, *223*, 24–38. [CrossRef]
35. Lai, S.; Xie, Z.; Bueh, C.; Gong, Y. Fidelity of the APHRODITE Dataset in Representing Extreme Precipitation over Central Asia. *Adv. Atmos. Sci.* **2020**, *37*, 1405–1416. [CrossRef]
36. Xia, Z.; Xinmin, W.; Han, L.I.; Linyi, L.Y.U. Construction and Application of Extreme Rainstorm Index Based on Environmental Parameters. *Meteor. Mon.* **2020**, *46*, 898–912.
37. Li, N.; Tang, G.; Zhao, P.; Hong, Y.; Gou, Y.; Yang, K. Statistical assessment and hydrological utility of the latest multi-satellite precipitation analysis IMERG in Ganjiang River basin. *Atmos. Res.* **2017**, *183*, 212–223. [CrossRef]
38. Ren, Z.; Zhao, P.; Zhang, Q.; Zhang, Z.; Chen, Z. Quality Control Procedures for Hourly Precipitation Data from Automatic Weather Stations in China. *Meteorol. Mon.* **2010**, *36*, 123–132.

39. Wu, W.; Zou, H.; Shan, J.; Wu, S. A Dynamical Z-R Relationship for Precipitation Estimation Based on Radar Echo-Top Height Classification. *Adv. Meteorol.* **2018**, *2018*, 8202031. [CrossRef]
40. Guo, H.; Chen, S.; Bao, A.; Behrangi, A.; Hong, Y.; Ndayisaba, F.; Hu, J.; Stepanian, P.M. Early assessment of Integrated Multi-satellite Retrievals for Global Precipitation Measurement over China. *Atmos. Res.* **2016**, *176*, 121–133. [CrossRef]
41. Li, X.; Chen, S.; Liang, Z.; Huang, C.; Li, Z.; Hu, B. Performance Assessment of GSMaP and GPM IMERG Products during Typhoon Mangkhut. *Atmosphere* **2021**, *12*, 134. [CrossRef]
42. Beck, H.E.; Pan, M.; Roy, T.; Weedon, G.P.; Pappenberger, F.; Van Dijk, A.I.J.M.; Huffman, G.J.; Adler, R.F.; Wood, E.F. Daily evaluation of 26 precipitation datasets using Stage-IV gauge-radar data for the CONUS. *Hydrol. Earth Syst. Sci.* **2019**, *23*, 207–224. [CrossRef]
43. Pan, Y.; Shen, Y.; Yu, J.; Zhao, P. Analysis of the combined gauge-satellite hourly precipitation over China based on the OI technique. *Acta Meteorol. Sin.* **2012**, *70*, 1381–1389.
44. Shen, Y.; Zhao, P.; Pan, Y.; Yu, J. A high spatiotemporal gauge-satellite merged precipitation analysis over China. *J. Geophys. Res.-Atmos.* **2014**, *119*, 3063–3075. [CrossRef]
45. Pan, Y.; Gu, J.; Xu, B.; Shen, Y.; Han, S.; Shi, C. Advances in multi-source precipitation merging research. *Adv. Meteorol. Sci. Technol.* **2018**, *8*, 143–152.
46. Yang, M.; Liu, G.; Chen, T.; Chen, Y.; Xia, C. Evaluation of GPM IMERG precipitation products with the point rain gauge records over Sichuan, China. *Atmos. Res.* **2020**, *246*, 105101. [CrossRef]
47. Tan, M.L.; Santo, H. Comparison of GPM IMERG, TMPA 3B42 and PERSIANN-CDR satellite precipitation products over Malaysia. *Atmos. Res.* **2018**, *202*, 63–76. [CrossRef]
48. Wang, W.; Lu, H.; Zhao, T.; Jiang, L.; Shi, J. Evaluation and Comparison of Daily Rainfall From Latest GPM and TRMM Products Over the Mekong River Basin. *IEEE J. Sel. Top. Appl. Earth Obs. Remote Sens.* **2017**, *10*, 2540–2549. [CrossRef]
49. Zhang, S.; Ma, Z.; Li, Z.; Zhang, P.; Liu, Q.; Nan, Y.; Zhang, J.; Hu, S.; Feng, Y.; Zhao, H. Using CYGNSS Data to Map Flood Inundation during the 2021 Extreme Precipitation in Henan Province, China. *Remote Sens.* **2021**, *13*, 5181. [CrossRef]
50. Jackson, G.; Petersen, W.; Berg, W.; Kidd, C.; Stocker, E.; Kirschbaum, D.; Kakar, R.; Braun, S.; Huffman, G.; Iguchi, T.; et al. The Global Precipitation Measurement (GPM) Mission for Science and Society. *Bull. Am. Meteorol. Soc.* **2017**, *98*, 1679–1695. [CrossRef]
51. Jiang, Q.; Li, W.; Fan, Z.; He, X.; Sun, W.; Chen, S.; Wen, J.; Gao, J.; Wang, J. Evaluation of the ERA5 reanalysis precipitation dataset over Chinese mainland. *J. Hydrol.* **2021**, *595*, 125660. [CrossRef]
52. Sun, H.; Yao, T.; Su, F.; He, Z.; Tang, G.; Li, N.; Zheng, B.; Huang, J.; Meng, F.; Ou, T.; et al. Corrected ERA5 precipitation by machine learning significantly improved flow simulations for the third pole basins. *J. Hydrometeorol.* **2022**, *23*, 1663–1679. [CrossRef]
53. Veloria, A.; Perez, G.J.; Tapang, G.; Comiso, J. Improved Rainfall Data in the Philippines through Concurrent Use of GPM IMERG and Ground-Based Measurements. *Remote Sens.* **2021**, *13*, 2859. [CrossRef]
54. Chen, S.; Hong, Y.; Kulie, M.; Behrangi, A.; Stepanian, P.M.; Cao, Q.; You, Y.; Zhang, J.; Hu, J.; Zhang, X. Comparison of snowfall estimates from the NASA CloudSat Cloud Profiling Radar and NOAA/NSSL Multi-Radar Multi-Sensor System. *J. Hydrol.* **2016**, *541*, 862–872. [CrossRef]
55. Dinku, T.; Chidzambwa, S.; Ceccato, P.; Connor, S.J.; Ropelewski, C.F. Validation of high-resolution satellite rainfall products over complex terrain. *Int. J. Remote Sens.* **2008**, *29*, 4097–4110. [CrossRef]
56. Islam, M.A.; Cartwright, N. Evaluation of climate reanalysis and space-borne precipitation products over Bangladesh. *Hydrol. Sci. J.* **2020**, *65*, 1112–1128. [CrossRef]
57. Wu, G.; Qin, S.; Mao, Y.; Ma, Z.; Shi, C. Validation of precipitation events in ERA5 to gauge observations during warm seasons over eastern China. *J. Hydrometeorol.* **2022**, *23*, 807–822. [CrossRef]
58. Lee, H.; Waliser, D.E.; Ferraro, R.; Iguchi, T.; Peters-Lidard, C.D.; Tian, B.; Loikith, P.C.; Wright, D.B. Evaluating hourly rainfall characteristics over the US Great Plains in dynamically downscaled climate model simulations using NASA-Unified WRF. *J. Geophys. Res.-Atmos.* **2017**, *122*, 7371–7384. [CrossRef]
59. Liu, S.N.; Wang, J.; Wang, H.J. Assessing 10 satellite precipitation products in capturing the July 2021 extreme heavy rain in Henan, China. *J. Meteor. Res.* **2022**, *36*, 798–808. [CrossRef]
60. Prakash, S.; Mitra, A.K.; Rajagopal, E.N.; Pai, D.S. Assessment of TRMM-based TMPA-3B42 and gsmap precipitation products over India for the Peak Southwest Monsoon season. *Int. J. Climatol.* **2015**, *36*, 1614–1631. [CrossRef]
61. Dullaart, J.C.; Muis, S.; Bloemendaal, N.; Aerts, J.C. Advancing global storm surge modelling using the new ERA5 climate reanalysis. *Clim. Dyn.* **2019**, *54*, 1007–1021. [CrossRef]
62. Wu, H.; Yong, B.; Shen, Z. Research on the Monitoring Ability of Fengyun-Based Quantitative Precipitation Estimates for Capturing Heavy Precipitation: A Case Study of the "7·20" Rainstorm in Henan Province, China. *Remote Sens.* **2023**, *15*, 2726. [CrossRef]
63. Li, S.; Huang, X.; Wu, W.; Du, B.; Jiang, Y. Evaluation of CMPAS precipitation products over Sichuan, China. *Atmos. Ocean. Sci. Lett.* **2022**, *15*, 100129. [CrossRef]
64. Gentilucci, M.; Barbieri, M.; Pambianchi, G. Reliability of the IMERG product through reference rain gauges in central Italy. *Atmos. Res.* **2022**, *278*, 106340. [CrossRef]
65. Seo, D.J.; Breidenbach, J.P. Real-time correction of spatially nonuniform bias in radar rainfall data using rain gauge measurements. *J. Hydrometeorol.* **2002**, *3*, 93–111. [CrossRef]

66. Hong, Y.; Hsu, K.L.; Sorooshian, S.; Gao, X. Precipitation estimation from remotely sensed imagery using a nartificial neural net-work cloud classification system. *J. Appl. Meteor.* **2004**, *43*, 1834–1853. [CrossRef]
67. Huffman, G.J.; Bolvin, D.T.; Nelkin, E.J.; Wolff, D.B.; Adler, R.F.; Gu, G.; Hong, Y.; Bowman, K.P.; Stocker, E.F. The TRMM multisatellite precipitation analysis (TMPA): Quasi-global, multiyear, combined-sensor precipitation estimates at finescales. *J. Hydrometeorol.* **2007**, *8*, 38–55. [CrossRef]